nature metabolism

Article

https://doi.org/10.1038/s42255-022-00638-1

GAB functions as a bioenergetic and signalling gatekeeper to control T cell inflammation

Received: 7 February 2022

Accepted: 12 August 2022

Published online: 3 October 2022

Check for updates

Siwen Kang[1], Lingling Liu[1], Tingting Wang[1], Matthew Cannon[1], Penghui Lin[2], Teresa W.-M. Fan[2], David A. Scott[3], Hsin-Jung Joyce Wu[4], Andrew N. Lane[2] and Ruoning Wang[1]

γ-Aminobutyrate (GAB), the biochemical form of (GABA) γ-aminobutyric acid, participates in shaping physiological processes, including the immune response. How GAB metabolism is controlled to mediate such functions remains elusive. Here we show that GAB is one of the most abundant metabolites in $CD4^+$ T helper 17 (T_H17) and induced T regulatory (iT_{reg}) cells. GAB functions as a bioenergetic and signalling gatekeeper by reciprocally controlling pro-inflammatory T_H17 cell and anti-inflammatory iT_{reg} cell differentiation through distinct mechanisms. 4-Aminobutyrate aminotransferase (ABAT) funnels GAB into the tricarboxylic acid (TCA) cycle to maximize carbon allocation in promoting T_H17 cell differentiation. By contrast, the absence of ABAT activity in iT_{reg} cells enables GAB to be exported to the extracellular environment where it acts as an autocrine signalling metabolite that promotes iT_{reg} cell differentiation. Accordingly, ablation of ABAT activity in T cells protects against experimental autoimmune encephalomyelitis (EAE) progression. Conversely, ablation of $GABA_A$ receptor in T cells worsens EAE. Our results suggest that the cell-autonomous control of GAB on $CD4^+$ T cells is bimodal and consists of the sequential action of two processes, ABAT-dependent mitochondrial anaplerosis and the receptor-dependent signalling response, both of which are required for T cell-mediated inflammation.

Mounting a robust and effective adaptive immune response in vertebrates is metabolically costly and requires proper allocation of essential yet limited energy and carbon resources. Metabolism must be tightly controlled at the cellular level to coordinate rapid expansion followed by a fine-tuned differentiation process in T cells. Beyond acting as bioenergetic substrates and biosynthetic precursors, metabolites can directly control cellular signalling responses through influencing DNA, RNA and protein modifications, signalling receptors' activities and the production of reactive oxygen species[1–5]. As such, metabolism is fundamental to fine-tuning carbon and nitrogen allocation and optimizing immune response, which is at the centre of many diseases. Previous studies have used systemic approaches to comprehensively

[1]Center for Childhood Cancer & Blood Diseases, Hematology/Oncology & BMT, Abigail Wexner Research Institute at Nationwide Children's Hospital, Department of Pediatrics at The Ohio State University, Columbus, OH, USA. [2]Center for Environmental and Systems Biochemistry, Department of Toxicology and Cancer Biology, Markey Cancer Center, University of Kentucky, Lexington, KY, USA. [3]Cancer Metabolism Core, Sanford Burnham Prebys Medical Discovery Institute, La Jolla, CA, USA. [4]Division of Rheumatology and Immunology, Department of Internal Medicine at The Ohio State University, Columbus, OH, USA. e-mail: ruoning.wang@nationwidechildrens.org

characterize the transcriptome, the abundance of intracellular metabolites and the overall catabolic activities of T cells at the different stages during the T cell life cycle[6,7]. These studies have generated critical temporal snapshots of the metabolic landscapes, which help establish a conceptual foundation for understanding T cell metabolic reprogramming. However, most of these studies have centred mainly on intracellular metabolites and activities of the central carbon metabolism. The overall metabolic landscape of T cells can also be delineated by monitoring the metabolites consumed from and secreted into the growth medium. The extracellular metabolome represents the ultimate outcome of metabolic input, processing and output. Extracellular metabolome profiling (also called metabolic footprinting) has been applied as a standard technique to optimize microbial bioprocesses by analysing substrates consumed from and metabolites secreted into a microorganism's culture medium[8,9]. Here, we took a similar approach (Fig. 1a) to compare the extracellular metabolome profiles of naive T (T_{nai}) cells and different subsets of effector T (T_{eff}) cells, including T helper (T_H0, T_H1, T_H17) cells and induced regulator T (iT_{reg}) cells.

Results

GAB is an abundant metabolite produced by effector T cells

The control (blank) medium and the spent medium of different subsets of T_{eff} cells (Extended Data Fig. 1a) were profiled on a semi-quantitative untargeted global metabolomics platform based on liquid chromatography–mass spectrometry (LC–MS), with broad coverage of up to 1,000–2,500 compounds, including amino acids, energy metabolites, nucleotides and lipids. Using this approach, we have classified metabolites as having changes in production or consumption according to whether the fold change compared with control was positive or negative, respectively. Hierarchical clustering analysis, the pairwise comparison and the principal-component analysis revealed that T cell subsets were characterized by distinct extracellular metabolome profiles (Fig. 1b and Extended Data Fig. 1b–g). Consistent with the role of central carbon metabolism in supporting cell growth, the hyper-proliferative T_{eff} groups consumed more carbohydrates and produced more lactate than the T_{nai} group (Extended Data Fig. 1e). Additionally, the T_H17 group was characterized by the highest production of polyamines (Fig. 1b), in line with the recent finding of a critical role for polyamine in determining T_H17 differentiation[10–12]. Intriguingly, iT_{reg} cells produced high levels of γ-aminobutyrate (GAB) and its derivatives (Fig. 1b). Next, we applied gas chromatography–MS (GC–MS)-based targeted metabolomics and nuclear magnetic resonance (NMR) to validate and quantify intracellular and extracellular GAB production. We confirmed that iT_{reg} cells produced much higher levels of GAB than T_H17 cells (Fig. 1c–h). Unexpectedly, GAB was the most abundant intracellular metabolite and among the top three extracellular metabolites in iT_{reg} cells (Fig. 1c,d). However, neither prolonged culture nor restimulation would significantly changed GAB excretion (Extended Data Fig. 1h,i). Following activation, thymus-derived T_{reg} (tT_{reg}) cells could also excrete a comparable amount of GAB to the medium as iT_{reg} cells (Fig. 1i). Notably, the intracellular level of GAB was even higher than that of glutamate (Glu) in iT_{reg} cells, which is one of the most abundant intracellular metabolites in various organisms[13]. GAB is produced by catabolizing glutamine (Gln) through the (GABA) γ-aminobutyric acid shunt and elicits GABAergic response through GABA receptors (GABA-Rs) in neurons. To better understand the molecular nature that determines GAB production and function in T cells, we examined the expression of a panel of GABA-related metabolic and receptor genes by qPCR (Fig. 1e,f). Consistent with the previous findings on the GABA-R expression profile in immune cells[14]. T_{eff} cells expressed a selected group of GABA-R subunits. However, only iT_{reg} and T_H17 cells expressed high levels of glutamate decarboxylase (GAD), the enzyme that catalyzes the decarboxylation of Glu to GAB. Unexpectedly, the T_H17 group exhibits a higher level of GAD than the iT_{reg} group and was the only group that expressed a high level of the GAB-catabolizing enzyme 4-aminobutyrate aminotransferase (ABAT), indicating increased GAB catabolism in T_H17 cells but not in iT_{reg} cells (Fig. 1f). Collectively, these findings suggest that extracellular metabolome profiling is a robust approach to revealing T cell metabolic characteristics in vitro. Using this approach, we have found that GAB is an abundant metabolite produced by T cells.

T cells use both Gln and Arg to produce GAB

Given the higher expression of GAD and ABAT in T_H17 cells relative to iT_{reg} cells, we reasoned that both iT_{reg} cells and T_H17 cells could produce GAB. However, the fate of GAB depends on ABAT, that is, GAB is diverted into the tricarboxylic acid (TCA) cycle in the presence of ABAT in T_H17 cells instead of being exported into the extracellular compartment in the absence of ABAT as in iT_{reg} cells. To test this idea, we cultured T_H17 cells with or without the potent ABAT inhibitor vigabatrin (Vig)[15,16], for 6 h and then measured the levels of a panel of metabolites. Inhibiting ABAT activity by Vig led to the accumulation of intracellular GAB and GAB release into the medium (Fig. 1k,j). Notably, inhibiting ABAT activity rendered GAB one of the most abundant metabolites in the medium and cell pellet (Fig. 1k,j). Moreover, we have validated that ABAT was expressed in T_H17 cells but not in iT_{reg} cells using immunoblot (IB) analysis and intracellular staining (Fig. 2a,b). Interestingly, inhibiting ABAT activity reduced Gln consumption without changing Glu levels significantly but increased GAB levels over 100-fold (Fig. 2c,d). The reciprocal changes in Gln consumption versus GAB production raise the possibility of a Gln-independent GAB production route in T_H17 cells. Gln catabolism via the GABA shunt is the canonical GAB biosynthesis pathway[17]. Alternatively, GAB could be formed from putrescine (Put), a metabolite mainly derived from arginine (Arg) (Fig. 2d)[18,19]. Indeed, the metabolic genes involved in converting Arg into GAB were highly expressed in T_H17 cells (Fig. 2e). To determine to what extent Gln and Arg contribute to GAB biosynthesis, we cultured T_H17 cells with Vig in the presence or absence of Gln, Arg or both. Then, we collected spent medium to measure the levels of various metabolites. While removing Gln or Arg reduced GAB production, the removal of both completely blocked GAB production (Fig. 2f). Next, we supplied [$^{13}C_6$]Arg, [$^{13}C_5$]Gln, [$^{13}C_6$]glucose (Glc) or [$^{13}C_4$]Put as metabolic tracers in the culture medium and followed ^{13}C incorporation into individual metabolites by GC–MS. The presence of the $^{13}C_4$ isotopologue of GAB and the corresponding $^{13}C_4$ or $^{3}C_5$ isotopologues of upstream metabolites further confirmed that Gln and Arg are carbon donors of GAB (Fig. 2g). However, only the $^{13}C_2$ isotopologue of GAB was detected in samples with [$^{13}C_6$]Glc, suggesting that Glc can support Glu (and GAB) synthesis through the TCA cycle (Fig. 2h). Finally, we showed that Put can be converted to GAB via a diamine oxidase (DAO)-dependent reaction as its inhibitor aminoguanidine (AG) completely blocked the production of [$^{13}C_4$]GAB from [$^{13}C_4$]Put (Fig. 2i). In addition to a general requirement of both amino acids for protein synthesis, we envisioned that Gln and Arg might also support T_H17 function and survival through supporting GAB biosynthesis. To test this idea, we cultured T_H17 cells in Gln/Arg-replete medium or suboptimal medium (with low levels of Gln/Arg) in the absence or presence of high levels of GAB. Supporting our hypothesis, reducing the amount of either amino acid led to defects in the maintenance of viability and interleukin (IL)-17$^+$ populations. Notably, GAB supplementation could correct both defects (Fig. 2j,k). We, therefore, conclude that T_H17 cells can use both Gln-derived and Arg-derived carbon to synthesize GAB and support cell viability and function.

ABAT confers GAB-dependent anaplerosis on T_H17 cells

Next, we reasoned that the expression of ABAT may render T_H17 cells capable of diverting GAB into the TCA cycle in a way that maximizes carbon allocation and oxidative phosphorylation (OXPHOS) in mitochondria. To test this idea, we added [$^{13}C_4$]GABA as a metabolic tracer into the culture medium and followed ^{13}C incorporation into intermediate metabolites of the TCA cycle in iT_{reg} cells and T_H17 cells with or

https://doi.org/10.1038/s42255-022-00638-1

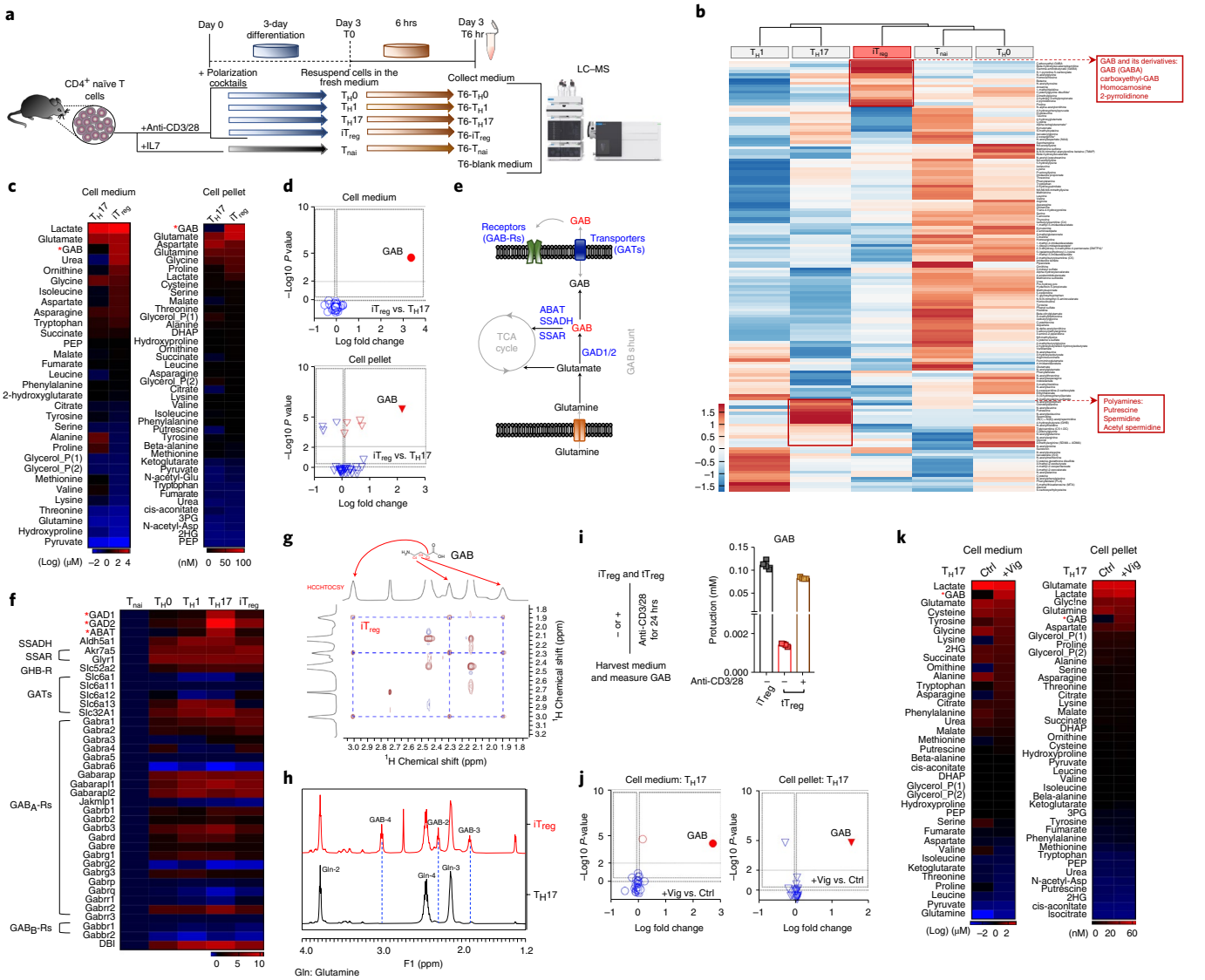

Fig. 1 | GAB is an abundant metabolite produced in T_H17 and iT_{reg} cells. **a**, Experimental scheme of T cell extracellular metabolome profiles (LC–MS). **b**, Extracellular metabolites associated with amino acid metabolism in the indicated T cell subsets were profiled by LC–MS. The value for each metabolite represents $n = 3$ biologically independent samples. The heatmap represents the value of the relative amount (see colour scale). The complete metabolomic profile is provided as source data. **c**,**d**,**j**,**k**, Indicated metabolites were quantified by GC–MS. The value for each metabolite represents $n = 3$ biologically independent samples. Cysteinylglycine disulfide*, (2R)-2-amino-3-{[2-amino-2-(carboxymethylcarbamoyl)ethyl]disulfanyl}propanoic acid; alpha-ketoglutaramate*, 2-keto-glutaramate; 2-oxoarginine*, 5-[(diaminomethylidene) amino]-2-oxopentanoic acid; 2,3-dihydroxy-5-methylthio-4-pentenoate (DMTPA)*, (2R,3R,4E)-2,3-dihydroxy-5-(methylsulfanyl)pent-4-enoic acid. The heatmaps (**c**,**k**) represent the log value (medium) or the absolute value (pellet) of the indicated metabolite quantity (see colour scale). The complete data are provided as source data. The volcano plots (**d**,**j**) show changes in metabolites in the cell medium and cell pellet. Heatmaps and volcano plots are representative of $n = 3$ independent biological samples from $n = 2$ independent biological experiments. **e**, Schematic of the pathway of GABA metabolism. **f**, RNA was isolated from the indicated T cell subsets ($n = 3$ biologically independent samples) and used for qPCR analyses of the indicated metabolic genes. mRNA levels of T_{nai} cells were set to 1. The heatmap represents the log value of the relative mRNA expression level (see colour scale). Values and s.d. are provided as source data. **g**,**h**, GAB in the indicated groups was determined and quantified by NMR ($n = 3$ biologically independent samples). **i**, As illustrated by the experimental scheme (left), GAB production in iT_{reg} and tT_{reg} cells was quantified by a GAB bioassay kit ($n = 4$ biologically independent samples). Statistical analysis was performed by R (**b**) or unpaired two-tailed Student's *t*-test (**c**,**d**,**i**–**k**). GAD, glutamate decarboxylase; SSADH, succinic semialdehyde dehydrogenase; SSAR, succinic semialdehyde reductase; GHB-R, γ-hydroxybutyrate receptor; GATs, GABA transporters; VGAT, vesicular GABA transporter; $GABA_A$-R, GABA type A receptor; $GABA_B$-R, GABA type B receptors; DBI, diazepam binding inhibitor.

without Vig treatment (Fig. 3a,b). In line with the expression of ABAT in T_H17 cells but not in iT_{reg} cells, T_H17 cells exhibited much higher levels of the $^{13}C_4$ isotopologue of succinate and its downstream metabolites in the TCA cycle than iT_{reg} cells (Fig. 3a). Inhibiting ABAT activity by Vig completely abolished the $^{13}C_4$ isotopologue of succinate and its downstream metabolites in T_H17 cells, supporting the idea that GAB is diverted to the TCA cycle via an ABAT-dependent reaction (Fig. 3b). Next, we sought to determine the temporal change in respiration following a sequential supplementation of GABA, Vig, oligomycin or carbonyl cyanide-*p*-trifluoromethoxyphenylhydrazone (FCCP) into the T_H17 cell culture medium. Indeed, GABA supplementation enhanced oxygen consumption in an ABAT-dependent manner, while ATPase inhibitor oligomycin suppressed and FCCP maximized oxygen consumption as expected (Fig. 3c). We and others have recently shown

https://doi.org/10.1038/s42255-022-00638-1

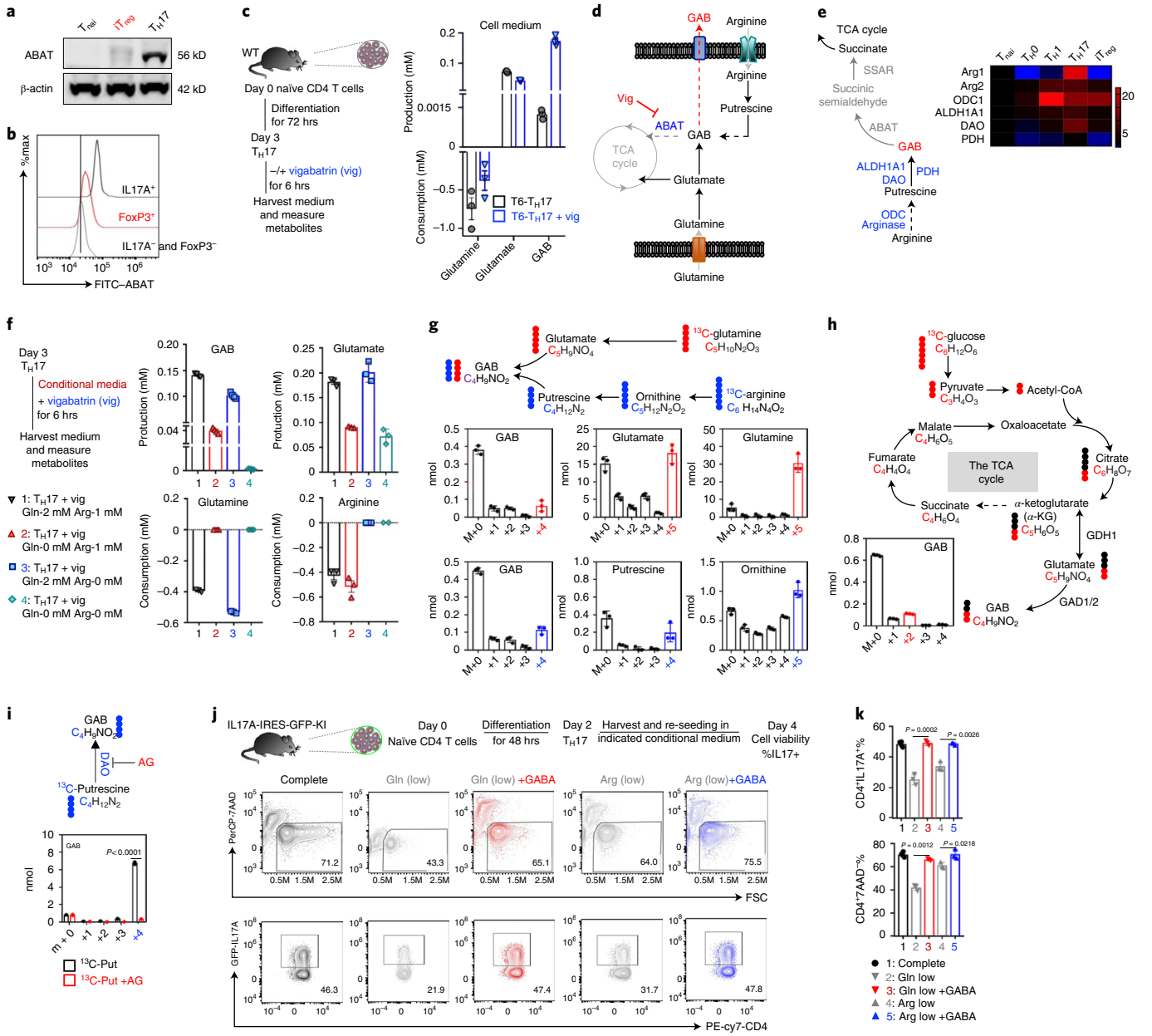

Fig. 2 | Gln and Arg are the main carbon sources for GAB biosynthesis in T_{eff} cells. a,b, ABAT protein levels were determined by IB (ABAT molecular weight, 56 kDa; full-scan images are provided as source data) (**a**) and cytometry (**b**). **c**, As illustrated by the experimental scheme (left), the indicated metabolites in T_H17 cells were quantified by GC–MS (right); data are representative of $n = 3$ biologically independent samples. **d**, Scheme of the GAB metabolic pathways and a pharmacological inhibitor Vig of ABAT. **e**, Schematic diagram of GAB biosynthesis from Arg (left), with the expression of relevant genes determined by qPCR detection (right). mRNA levels for T_{nai} cells were set to 1. The heatmap represents the relative mRNA expression level (see colour scale). Values and s.d. are provided as source data. **f**. As illustrated by the experimental scheme (left), the indicated metabolites in T_H17 cells were quantified by YSI (Gln and Glu) or by bioassay kits (Arg and GAB) ($n = 3$ biologically independent samples). **g**, Diagram of conversion of [$^{13}C_5$]Glu and [$^{13}C_6$]Arg to downstream metabolites (top). Indicated metabolites in T_H17 cells were quantified by GC–MS ($n = 3$ biologically independent samples) (bottom). Numbers along the *x* axis represent those of ^{13}C atoms in the given metabolites. **h**, Diagram of the conversion of [$^{13}C_6$]Glc to downstream metabolites. Indicated metabolites in T_H17 cells were quantified by GC–MS ($n = 3$ biologically independent samples). Black dot, ^{12}C; red dot, ^{13}C derived from [$^{13}C_6$]Glc. **i**, Diagram of the conversion of [$^{13}C_4$]Put to GAB. Indicated metabolites in T_H17 cells were quantified by GC–MS ($n = 3$ biologically independent samples). Unpaired two-tailed Student's *t*-test. **j**, As illustrated by the experimental scheme (top), cytokine expression and cell viability were determined by flow cytometry (bottom). All experiments with bicuculline (5 μM); complete medium, 2 mM Gln + 0.1 mM Arg; Gln (low), 10 μM Gln + 0.1 mM Arg; Gln (low plus GABA), 10 μM Gln + 0.1 mM Arg + 1 mM GABA; Arg (low), 2 mM Gln + 10 μM Arg; Arg (low plus GABA) 2 mM Gln + 10 μM Arg + 1 mM GABA. **k**, Statistical analysis for **j**; data are representative of $n = 3$ biologically independent samples. Significance was calculated by one-way ANOVA with Tukey's multiple-comparisons test. Gln, glutamine; Glu, glutamate; Arg, arginine; ODC, ornithine decarboxylase; DAO, diamine oxidase; PDH, pyrroline dehydrogenase; M, million.

that Arg-dependent polyamine biosynthesis is required to support T cell proliferation and T_H17 cell differentiation[10–12]. We reasoned that ABAT expression in T_H17 cells might allow Arg-derived carbons to be diverted into the TCA cycle through Put and GAB. Supporting this idea, [$^{13}C_6$]Arg-derived and [$^{13}C_4$]Put-derived ^{13}C were incorporated into the $^{13}C_4$ isotopologue of succinate and its downstream metabolites in an ABAT-dependent manner in T_H17 cells (Fig. 3d, e). Finally, we sought to determine whether Gln-derived carbons could enter the TCA cycle via

https://doi.org/10.1038/s42255-022-00638-1

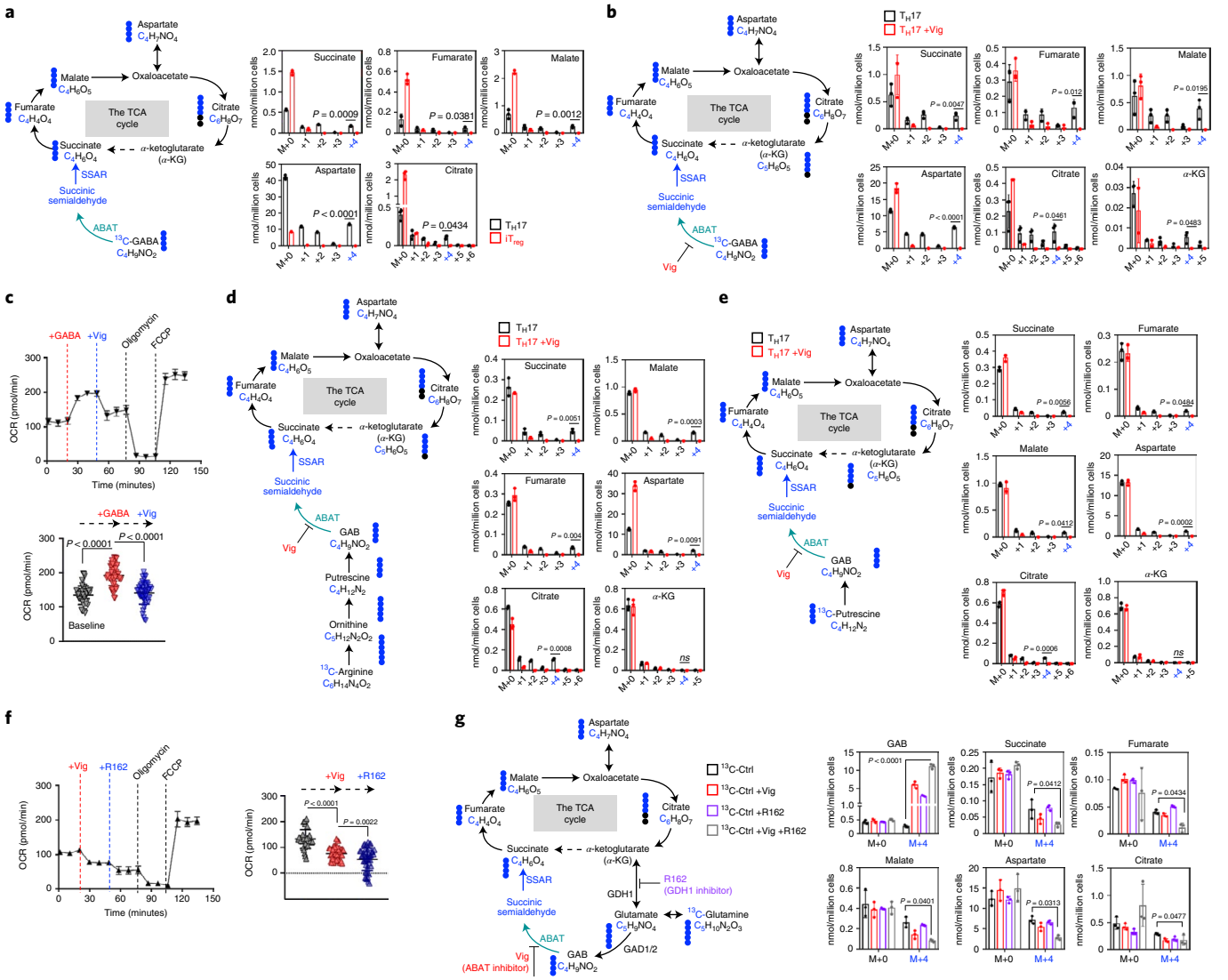

Fig. 3 | ABAT enables diversion of GAB into the TCA cycle in T cells. **a**,**b**,**c**,**d**,**e**,**g**, Diagrams of the conversion of [$^{13}C_4$]GABA (**a**,**b**, left), [$^{13}C_6$]Arg (**d**, left), [$^{13}C_4$]Put (**e**, left) and [$^{13}C_5$]Gln (**g**, left) to downstream metabolites. Indicated metabolites in T_H17 cells were quantified by GC–MS ($n = 3$ biologically independent samples) (right). Black dot, ^{12}C; blue dot, ^{13}C derived from the indicated tracers. Numbers along the *x* axis represent those of ^{13}C atoms in the given metabolites. Significance was calculated by unpaired two-tailed Student's *t*-test (**a, b, d, e** and **g**); NS, no significant differences. **c,f**, OCR of T_H17 cells with the indicated treatments was determined by Seahorse. Data are representative of $n = 16$ independent biological samples from $n = 3$ independent biological experiments. Two-way ANOVA with Sidak's multiple-comparisons test (**c**) and (**f**). α-KG, α-ketoglutarate; GDH, glutamate dehydrogenase.

ABAT. Gln is a major carbon donor known to drive the TCA cycle and OXPHOS via glutamine transaminase and glutamate dehydrogenase (GDH) in T_{eff} cells[20–22]. We found that a sequential supplementation with Vig and the GDH inhibitor R162 (ref. [23]) suppressed oxygen consumption additively (Fig. 3f). Similarly, combining Vig and R162 suppressed [$^{13}C_5$]Gln-derived ^{13}C incorporation into the TCA cycle metabolites more profoundly than single-agent treatment (Fig. 3g). Collectively, we have identified GAB as a conditional anaplerotic substrate in T cells, and its catabolism via the TCA cycle depends on the expression of ABAT.

GAB metabolism controls proliferation and differentiation

To further delineate the role of ABAT in T cells, we generated a T cell-specific *Abat*-knockout strain (*Abat* cKO) by crossing the *Abat*^{fl} strain with the Cd4-Cre strain. qPCR, IB and intracellular staining analyses validated the deletion of ABAT (Fig. 4a, b). ABAT deletion did not result in T cell development defects in the thymus, the spleen or lymph nodes (Extended Data Fig. 2a–f). In addition, ABAT deletion did not affect cell viability, the expression of cell surface activation markers, the cell cycle progression from G0/G1 to the S phase, RNA, DNA or protein contents, cell size, or viability 24 h after activation in vitro (Extended Data Fig. 3a–d). However, ABAT deletion moderately suppressed overall T cell proliferation after activation in vitro (Fig. 4c and Extended Data Fig. 3e). Remarkably, both genetic and pharmacological ablation of ABAT activity inhibited pro-inflammatory T_H17 cell differentiation while enhancing anti-inflammatory iT_{reg} cell differentiation in vitro (Fig. 4c). Supporting these findings, the RNA-seq analysis of wild-type (WT) and *Abat* cKO T cells activated under the T_H0 condition revealed enriched gene signatures associated with inflammation and T cell differentiation (Fig. 4d–f). Notably, the ABAT inhibitor (Vig) did not potentiate the effect of genetic deletion in suppressing T_H17 cell differentiation, suggesting that Vig is a specific inhibitor of ABAT (Extended Data Fig. 4a). Moreover, overexpressing ABAT (ABAT-OE) suppressed iT_{reg} differentiation and could synergize with IL-6 to increase the percentage of IL-17$^+$ cells under the iT_{reg}-polarizing condition in vitro (Extended Data Fig. 4b). Next, we examined the effect of ABAT inhibition on T_H1 and T_H2 differentiation. Genetic and pharmacological ablation of ABAT

https://doi.org/10.1038/s42255-022-00638-1

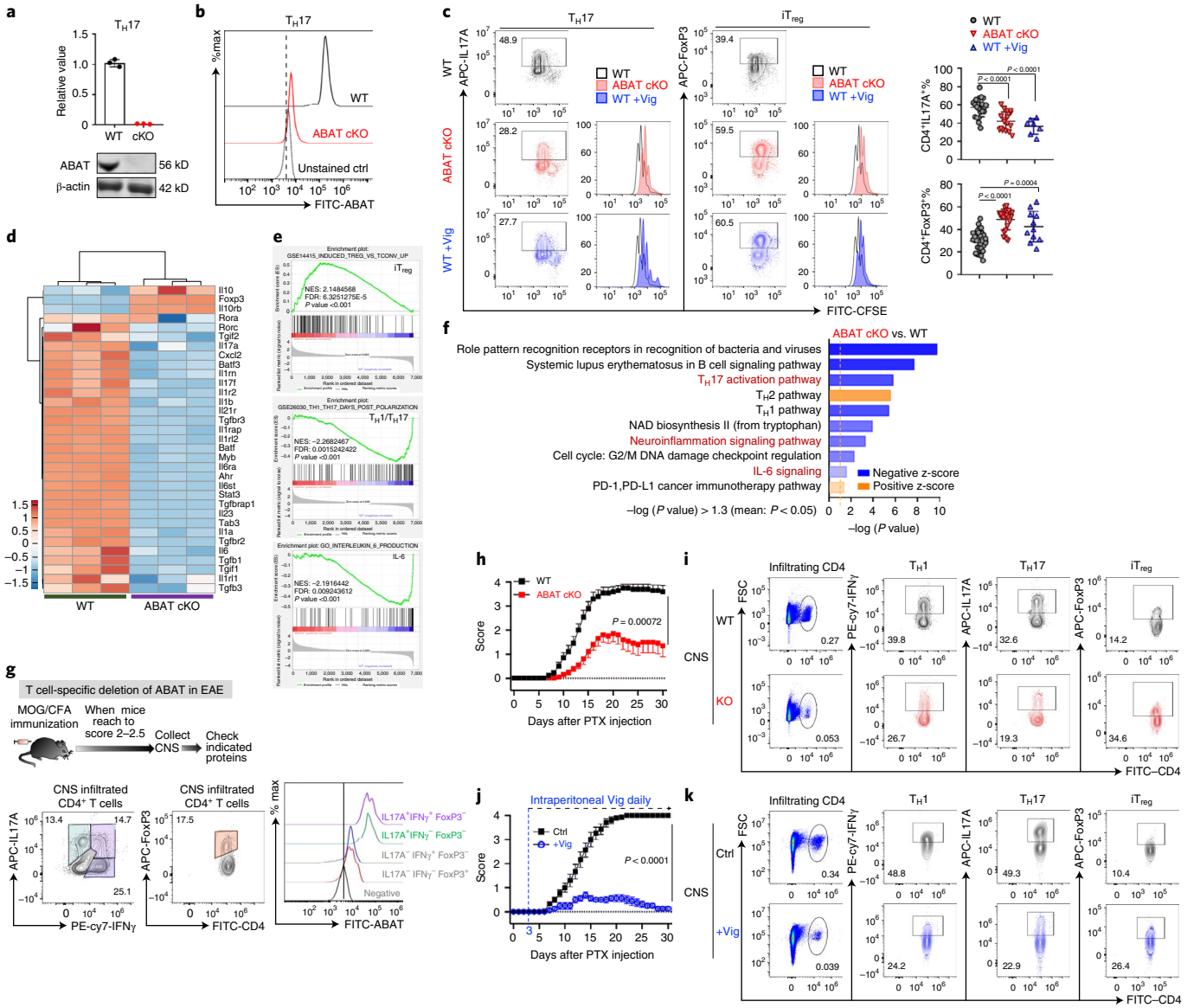

Fig. 4 | Genetic ablation or pharmacological inhibition of ABAT suppresses T_H17 but enhances iT_{reg} cell differentiation. a,**b**, ABAT mRNA and protein levels were determined by qPCR and IB analysis (**a**, full-scan images are provided in as source data) or by flow cytometry (**b**); unpaired two-tailed Student's *t*-test for **a** ($n = 3$ biologically independent samples). **c**, Expression of the indicated cytokines and CFSE dilution in the indicated groups determined by flow cytometry (WT, $n = 5$ independent biological samples from $n = 5$ independent biological experiments; *Abat* cKO, $n = 5$ independent biological samples from $n = 3$ independent biological experiments; WT plus Vig, $n = 3$ independent biological samples from $n = 3$ independent biological experiments). Two-way ANOVA with Sidak's multiple-comparisons test. **d**–**f**, Hierarchical clustering analysis, gene set enrichment analysis (GSEA) and Ingenuity Pathway Analysis (IPA) of a list of inflammatory genes performed by using RNA-seq data of $CD4^+$ T cells that were cultured under T_H0 culture conditions and collected at 36 h after activation ($n = 3$ independent biological samples). In **d**, heatmaps represent the log-transformed value of the quantity (see colour scale). In **f**, the orange dotted line along the *x* axis indicates the cut-off value ($P = 0.05$). The complete data are provided as source data. **g**, As illustrated by the experimental scheme (top), the expression of the indicated proteins in CNS-infiltrating $CD4^+$ T cells isolated from EAE animals was determined by flow cytometry ($n = 3$ independent biological samples from $n = 2$ independent biological experiments). **h**,**j**, EAE clinical scores in the indicated groups evaluated daily from mice of the indicated genotypes ($n = 6$ independent biological samples from $n = 2$ independent biological experiments in **h** and $n = 5$ independent biological samples from $n = 3$ independent biological experiments in **j**); significance was calculated by unpaired two-tailed Student's *t*-test. **i**,**k**, The expression of the indicated markers in CNS-infiltrating T cells determined by flow cytometry ($n = 5$ independent biological samples in **i** and $n = 3$ independent biological samples in **k**). PTX, paclitaxel; NES, normalized enrichment score; FDR, false discovery rate.

activity inhibited T_H1 cell differentiation without significantly changing T_H2 cell differentiation significantly in vitro (Extended Data Fig. 4c, d). Finally, we asked whether T_H1 cells could divert GAB into the TCA cycle as T_H17 cells did. We applied [$^{13}C_4$]GABA as a metabolic tracer and followed ^{13}C incorporation into intermediate metabolites of the TCA cycle in T_H1 and T_H17 cells. Only T_H17 cells exhibited high levels of the $^{13}C_4$ isotopologue of succinate and its downstream metabolites in the TCA cycle (Extended Data Fig. 4e). Notably, genetic and pharmacological ablation of ABAT activity completely abolished the $^{13}C_4$ isotopologues of metabolites in T_H17 cells (Extended Data Fig. 4e).

The expansion and balance between pro-inflammatory $CD4^+$ T_{eff} cells and anti-inflammatory $CD4^+$ T_{reg} cells determine the pathogenic development of experimental autoimmune encephalomyelitis (EAE), a mouse model of multiple sclerosis (MS), which is an inflammatory

demyelinating disease of the central nervous system (CNS). Consistent with the expression profile of ABAT in vitro, the IL-17$^+$CD4$^+$ T cell group expressed the highest level of ABAT among all the CD4$^+$ T subsets with infiltration into the CNS in animals with EAE (Fig. 4g). Notably, the genetic deletion of *Abat* in T cells or the systemic delivery of Vig conferred significant protection against EAE pathogenic progression, associated with more infiltrated FoxP3$^+$CD4$^+$ T cells and fewer infiltrated inflammatory CD4$^+$ T cells, reciprocally (Fig. 4h,i and Extended Data Fig. 5a,b). However, Vig treatment resulted in better protection against EAE and a broader impact on periphery CD4$^+$ T cells in the periphery than T cell-specific deletion of *Abat*, indicating that the systemic inhibition of ABAT might affect inflammation through both T cell-intrinsic and T cell-extrinsic mechanisms (Fig. 4j,k, and Extended Data Fig. 5c,d). We also used a competitive antigen-specific, T cell receptor (TCR)-dependent proliferation assay (OT-II) and a competitive homeostatic proliferation assay to assess T cell proliferation and differentiation in vivo. Notably, the ratio between WT and *Abat* cKO CD4$^+$ T cells, CFSE dilution patterns and the percentage of IL-17$^+$CD4$^+$ or interferon-γ (IFNγ$^+$)CD4$^+$ T cells in various tissues suggested that the loss of ABAT dampens T cell proliferation and T_H1 and T_H17 differentiation in vivo (Extended Data Fig. 6a–e). Collectively, our results indicate that ABAT status determines the fate of intracellular GAB and, hence, pro-inflammatory T_H17 and anti-inflammatory iT_{reg} cell differentiation in vitro and in vivo.

GAB regulates T cell differentiation through the $GABA_A$ receptor

In line with earlier studies[14], we have found that T_{eff} cells express various subunits of the $GABA_A$ receptor ($GABA_A$-R) (Fig. 1f). Additionally, T cells can produce and secrete a large amount of GAB into the extracellular compartment, which may elicit a context-dependent autocrine signalling response to regulate T cell differentiation (Fig. 5a). Supporting this idea, a low level of GAB supplementation could reduce T_H17 but enhance iT_{reg} differentiation without significantly affecting T cell activation and proliferation in vitro (Fig. 5b,c and Extended Data Fig. 7a,b). Conversely, $GABA_A$-R antagonists with distinct antagonistic mechanisms enhanced T_H17 cell differentiation but reduced iT_{reg} cell differentiation without affecting T cell activation and proliferation in vitro (Fig. 5c–e and Extended Data Fig. 7c,d). The β-subunit is a core component of $GABA_A$-R, and the β3 subunit (encoded by *Gabrb3*) was highly expressed in all T_{eff} subsets (Fig. 1f). We generated a T cell-specific *Gabrb3*-knockout strain (*Gabrb3* cKO) by crossing the *Gabrb3*^{fl} strain with the *CD4*-Cre strain. *Gabrb3* deletion did not result in T cell development defects in the thymus, spleen and lymph nodes (Extended Data Fig. 8a–f). In addition, cell viability, the expression of cell surface activation markers and cell proliferation were comparable in both WT and *Gabrb3* cKO T cells after activation in vitro (Extended Data Fig. 9a,b). However, genetic ablation of *Gabrb3* promoted pro-inflammatory T_H17 cell differentiation while reducing anti-inflammatory iT_{reg} cell differentiation in vitro (Fig. 5c,f). Notably, GABA supplementation only affected WT but not *Gabrb3* cKO T cell differentiation in vitro (Fig. 5c,f). Finally, the T cell-specific *Gabrb3* deletion let to significantly deteriorated EAE pathogenic progression, associated with increased inflammatory CD4$^+$ T cells and decreased FoxP3$^+$CD4$^+$ T cells in the CNS and periphery (Fig. 5g,h and Extended Data Fig. 9c,d).

GAB regulates T cells through a bimodal mechanism of action

Next, we sought to dissect the effect of ABAT-dependent mitochondrial anaplerosis and $GABA_A$-R-mediated signalling on T cell differentiation and function (Extended Data Fig. 10a). We envisioned that the ABAT-dependent anaplerotic reaction might support T_H17 differentiation by providing succinate to fuel mitochondrial OXPHOS (Fig. 6a). Indeed, inhibiting ABAT activity by Vig suppressed oxygen consumption, which was reversed by adding a cell-permeable succinate analogue NV118 (Fig. 6a,b)[24]. In line with the effect of NV118 on oxygen consumption, the NV118 supplementation could partially reverse the inhibition of T_H17 differentiation resulting from genetic or pharmacological inhibition of ABAT (Fig. 6c,d). Next, we asked whether ABAT-dependent mitochondrial anaplerosis could impact transcription factors critical for T_H17 lineage differentiation, such as RORγt and STATs[25]. To test this idea, we reduced the medium's Gln concentration and added a high concentration of GAB (1 mM) with a $GABA_A$-R antagonist. We reasoned that reducing Gln levels would force cells to use GAB as a mitochondrial fuel and adding the receptor antagonist would eliminate the effects of receptor signaling. Indeed, GAB supplementation significantly enhanced the levels of RORγt and phosphorylated STAT3 (pSTAT3) but reduced the levels of phosphorylated STAT5 (pSTAT5) (Extended Data Fig. 10b).

Next, we sought to determine whether modulating $GABA_A$-R affects key signalling molecules involved in regulating T_H17 and iT_{reg} differentiation. We treated T cells with a low dose of GAB (10 μM) in the presence of a $GABA_A$-R antagonist. We reasoned that the low dose of GAB could engage the receptor-mediated signalling response without significantly fuelling mitochondrial metabolism. We assessed the levels of phosphorylated STAT proteins and the phosphorylation of a canonical mTORC1 substrate (pS6) because mTORC1 is critical for determining T_H17 and iT_{reg} differentiation[26,27]. Treating T_H17 and iT_{reg} cells with a low dose of GAB suppressed pSTAT3 and mTORC1 substrate phosphorylation (pS6) but increased pSTAT5 (Extended Data Fig. 10c). Notably, the effects of GAB on these signalling molecules could be reversed by a $GABA_A$-R antagonist (Extended Data Fig. 10c). We showed that iT_{reg} cells can excrete GAB into the extracellular compartment (Extended Data Fig. 1g–i). Finally, we sought to determine whether GAB contributes to T_{reg}-dependent immune suppression. We performed a competitive T_{reg} suppression assay by co-culturing iT_{reg} cells with WT and *Gabrb3* cKO CD4$^+$ T cells that carried different isogenic markers (Fig. 6e). Indeed, *Gabrb3* cKO CD4$^+$ T cells proliferated better than the WT group, indicating that genetic ablation of $GABA_A$-R could partially alleviate iT_{reg}-mediated suppression (Fig. 6e). Together, these results suggest that GAB is an abundant metabolite produced by T cells and exerts both bioenergetic control and receptor-mediated signalling control of T cell differentiation (Fig. 6f).

Discussion

The vertebrate immune and nervous systems are intimately connected with each other developmentally, anatomically and physiologically. Interaction between the two systems coordinates their sensory functions to ensure organismal homeostasis and survival[28–31]. Immune cells and neurons can communicate with each other through a group of shared ligand molecules and receptors, including the neurotransmitter GABA and its receptors[14,32]. Beyond mediating intersystem communication between the immune and nervous systems, growing evidence suggests that GABA can also act as a paracrine signalling molecule mediating intrasystem communication to regulate immune response[33]. One recent study has found that B cells can produce GABA and suppress anti-tumour immunity through paracrine modulation of intratumoural macrophages and CD8$^+$ T cells[34]. Additionally, GABA in macrophages has been implicated as an intracellular metabolite with a pro-inflammatory function[14]. Here, we show that GAB (the biochemical form of GABA at physiological pH) is one of the most abundant metabolites in T cells and promotes inflammation through modulating T cell proliferation and differentiation. Depending on the status of its catabolizing enzyme ABAT, GAB can act as a conditional anaplerotic substrate to promote T_H17 cell differentiation or an autocrine signalling metabolite to enhance iT_{reg} cell differentiation. In addition to its role in mediating intercellular communications, GAB also serves as a metabolic and signalling gatekeeper to regulate inflammation in a T cell-autonomous manner.

T_{eff} cells consume Gln and Arg at high rates[35,36]. Beyond a general requirement for protein synthesis, Gln and Arg support T cell

https://doi.org/10.1038/s42255-022-00638-1

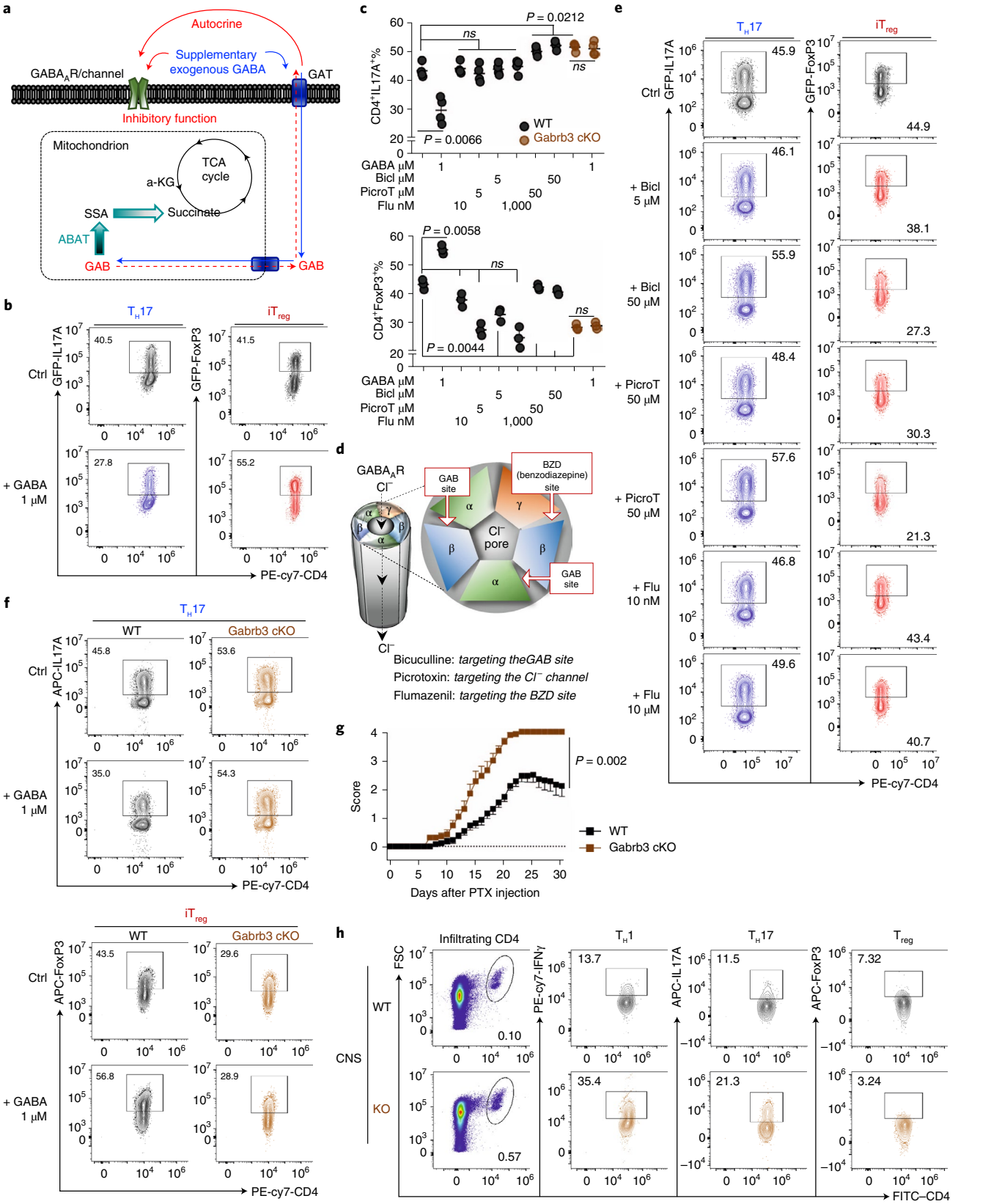

Fig. 5 | Receptor-mediated GAB autocrine signalling response reciprocally suppresses T_H17 and enhances iT_{reg} differentiation. a,**d**, Schematic diagram of GAB metabolism and the $GABA_A$-R-mediated autocrine signalling response in T cells (**a**) and schematic diagram of the binding sites for $GABA_A$-R antagonists (**d**). **b**,**e**,**f**, Cytokine expression of the indicated groups determined by flow cytometry. **c**, Combination statistical analysis of **b**, **e** and **f;** data are shown as mean ± s.e.m. ($n = 4$ independent biological samples). Significance was calculated by two-way ANOVA with Sidak's multiple-comparisons test. **g**, EAE clinical scores in the indicated groups evaluated daily ($n = 5$ independent biological samples from $n = 3$ independent biological experiments); significance was calculated by unpaired two-tailed Student's *t*-test. **h**, Expression of the indicated markers in CNS-infiltrating T cells were determined by flow cytometry ($n = 3$ independent biological samples). Bicl, bicuculline; PicroT, picrotoxin; Flu, flumazenil; PTX, paclitaxel.

https://doi.org/10.1038/s42255-022-00638-1

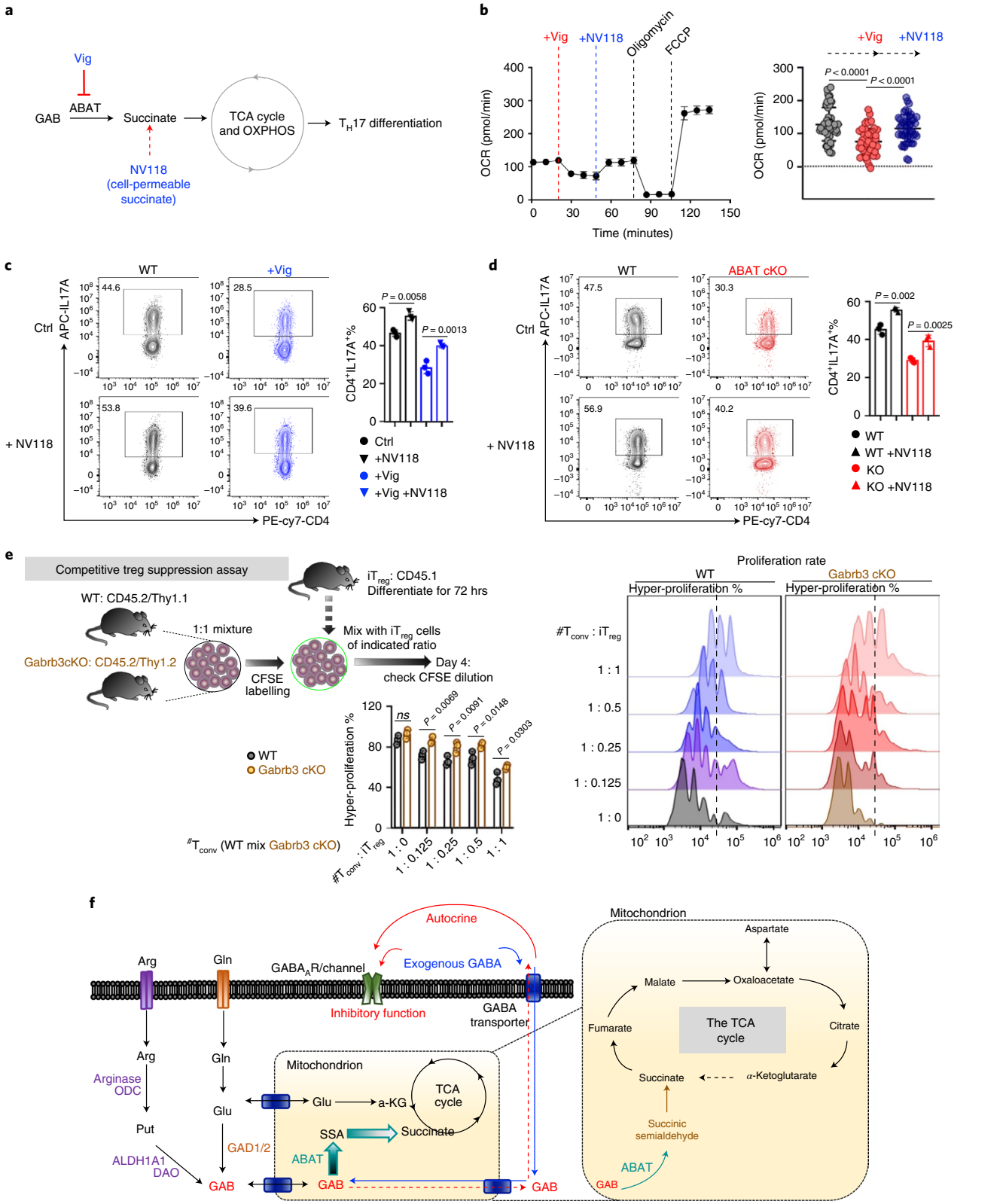

Fig. 6 | GAB exerts both bioenergetic and receptor signalling-mediated control of T cell differentiation. a, Schematic diagram of GAB catabolism through the TCA cycle. **b**, OCR of T_H17 cells with the indicated treatments determined by Seahorse ($n = 16$ independent biological samples from $n = 3$ independent biological experiments); significance was calculated by two-way ANOVA with Sidak's multiple-comparisons test. **c**,**d**, Expression of IL-17A in the indicated groups determined by flow cytometry ($n = 3$ independent biological samples); significance was determined by one-way ANOVA with Tukey's multiple-comparisons test. **e**, Left, experimental diagram of the competitive T_{reg} suppression assay. Right, CFSE dilution was determined by flow cytometry ($n = 3$ independent biological samples); significance was determined by two-way ANOVA with Sidak's multiple-comparisons test. **f**, Schematic conceptual model in which GAB generated by Gln and Arg can regulate T cell differentiation by entering the TCA cycle or being exporting into the extracellular environment and acting on $GABA_A$-R. T_{conv}, conventional T cells.

proliferation and function through their catabolic products. Gln is a primary carbon source to sustain the TCA cycle, which generates energy through OXPHOS and allocates carbon to produce biosynthetic precursors to support T cell growth[21,36,37]. Similarly, Arg catabolism is coupled with the urea cycle to produce bioactive metabolites such as polyamines to support T cell proliferation and differentiation[10–12]. Our results show that both Arg catabolism (via Put) and Gln catabolism (via Glu) are coupled with GAB biosynthesis in T_H17 cells, implicating GAB as a crucial metabolic node and a branch point in amino acid catabolism. GAB can be consumed through the TCA cycle to enhance bioenergetic and biosynthetic capacities or be secreted as an autocrine signalling metabolite depending on the status of ABAT. We have further revealed that Gln can replenish the TCA cycle intermediate metabolites through either Glu or GAB anaplerosis. Glu increases the levels of α-ketoglutarate (α-KG), while GAB increases the levels of succinate. Therefore, it is conceivable that the carbon input from Glu or GAB may change the intracellular α-KG to succinate ratio reciprocally. Hence, the GABA shunt in T cells may impact the hypoxia signalling response and/or DNA/histone methylation patterns by modulating the enzymatic activities of the α-KG-dependent dioxygenase family[37–40], and Glu and Put are highly abundant intracellular metabolites that can be secreted to the extracellular environment by T_H17 cells (Fig. 1a)[10,41]. The GAB-catabolizing enzyme ABAT may provide a sensitive and precise regulation of the three interconnected and highly abundant metabolites: GAB, Glu and Put, permitting rapid metabolic and signalling responses to control inflammation.

The high and dynamic metabolic demands of T cells during inflammatory and autoimmune responses require fine-tuned regulation of central carbon and ancillary metabolic pathways. Hence, metabolic pathways have been therapeutically exploited to target inflammatory and autoimmune diseases[42,43]. Disruption of central carbon catabolism can affect many cellular processes and cell types. However, targeting ancillary metabolic pathways engaged in a small group of specialized immune cells under physio-pathological conditions may result in less toxicity but maximal clinical benefits[6]. Gene and protein expression profiling studies have suggested that human autoimmune diseases, including MS, type 1 diabetes and rheumatoid arthritis, are associated with the dysregulation of GABA-related metabolic and signaling genes[44–47]. Interestingly, cortical GAB levels are lower in patients with relapsing–remitting multiple sclerosis MS than in healthy controls[48,49]. In addition, one recent study based on genome-scale metabolic modelling and in silico simulations for drug response indicated that GAB metabolism and signalling pathway not only are involved in the disease process but also are potential drug targets in human autoimmune diseases[50]. Consistent with clinical profiling and in silico studies, pharmacological modulation of GAB metabolism and receptor-mediated signalling response could ameliorate pathological phenotypes in several preclinical models of autoimmune diseases[51–55]. Our results further elucidate a previously unrecognized aspect of the T cell-intrinsic effects conferred by GAB catabolism and receptor-mediated signalling. Collectively, GAB-modulating strategies via blockade of GAB catabolism, activation of receptor-mediated response, or both may present a promising therapy for treating inflammatory and autoimmune diseases.

Methods

Mice

C57BL/6 (WT), Flippase (B6.129S4*Gt(ROSA)26Sor*$^{tm1(FLP1)Dym}$/RainJ), OT-II (B6.Cg-Tg(TcraTcrb)425Cbn/J), CD45.1$^+$ (B6.SJL-*Ptprc*^{a}*Pepc*^{b}/BoyJ), *Rag1*$^{-/-}$ (B6.129S7-*Rag1*^{tm1Mom}/J), IL17A-IRES-GFP-KI (C57BL/6-*Il17a*^{tm1Bcgen}/J), FoxP3^{GFP+} (C57BL/6-Tg(Foxp3-GFP)90Pkraj/J) and *Gabrb3*^{fl} (B6;129-*Gabrb3*$^{tm2.1Geh}$/J) mice were obtained from the Jackson Laboratory (JAX, Bar Harbor, ME). Mice with one targeted allele of *Abat* on the C57BL/6 background (*Abat*$^{tm1a(EUCOMM)Hmgu}$) were generated by the European Conditional Mouse Mutagenesis Program (EUCOMM)[56]. The mice were first crossed with a transgenic Flippase strain (B6.129S4*Gt(ROSA)26Sor*$^{tm1(FLP1)Dym}$/RainJ) to remove the *lacZ*-reporter allele and then crossed with the *Cd4*-Cre strain to generate the T cell-specific *Abat* knockout strain (*Abat* cKO). OT-II mice were crossed with *Cd4*-Cre *Abat* cKO mice to generate the OT-II *Cd4*-Cre *Abat* cKO mice. OT-II mice were crossed with *Thy1.1*$^+$ mice (B6.PL-*Thy1*^{a}/CyJ) to generate the OT-II *Thy1.1* mice. *Gabrb3*^{fl} mice were crossed with the *Cd4*-Cre strain to generate T cell-specific *Gabrb3*-knockout strain (*Gabrb3* cKO). For one independent experiment, we used male and female mice from the same strain that were both sex and age matched (6–12 weeks old), such as two males and two females for WT mice, as well as for KO mice. All mice were bred and kept in specific pathogen-free conditions at the Animal Center of the Abigail Wexner Research Institute at Nationwide Children's Hospital. A low-fat diet was provided (Envigo 2920, the irradiated form of 2020X; https://insights.envigo.com/hubfs/resources/ data-sheets/2020x-datasheet-0915.pdf). Animals were killed by carbon dioxide asphyxiation followed by cervical dislocation under protocols approved by the Institutional Animal Care and Use Committee of the Abigail Wexner Research Institute at Nationwide Children's Hospital (IACUC; protocol number AR13-00055).

Murine T cell isolation and culture

Naive CD4$^+$ T cells were enriched from mouse spleen and lymph nodes by negative selection using the MojoSort™ Mouse CD4$^+$ Naive T Cell Isolation Kit (MojoSort, BioLegend) according to the manufacturer's instructions. For the activation assay, freshly isolated CD4$^+$ T cells were either maintained in a culture medium with 5 ng/ml^{-1} IL-7 or activated with 5 ng/ml^{-1} IL-2 and plate-bound anti-mouse CD3 and anti-mouse CD28. The culture plates were precoated with 2 μg/ml^{-1} anti-mouse CD3 and 2 μg/ml^{-1} anti-mouse CD28 antibodies overnight at 4 °C. Naive tT_{reg} cells were enriched from mouse spleen and lymph nodes by positive selection using the MojoSort™ Mouse CD4$^+$CD25$^+$ Regulatory T Cell Isolation Kit (MojoSort, BioLegend) according to the manufacturer's instructions. For the activation assay, freshly isolated CD4$^+$CD25$^+$ regulatory T cells were either maintained in a culture medium with 5 ng/ml^{-1} IL-2 or activated with 5 ng/ml^{-1} IL-2 and anti-mouse CD3/CD28 beads according to the manufacturer's instructions (Gibco, Thermo Fisher Scientific). Unless indicated separately, the cells were seeded in the RPMI-1640 medium (Corning) supplemented with 10% FBS, or heat-inactivated dialysed FBS (DFBS), 2 mM L-glutamine, 1% sodium pyruvate (Sigma-Aldrich), 100 units/ml^{-1} penicillin, 100 μg/ml^{-1} streptomycin and 0.05 mM 2-mercaptoethanol (Sigma-Aldrich) at 37 °C and 5% CO_2.

For CD4$^+$ T cell differentiation, 48-well culture plates were precoated with 2 μg/ml^{-1} (iT_{reg} differentiation), 5 μg/ml^{-1} (T_H1/ T_H2 differentiation) or 10 μg/ml^{-1} (T_H17 differentiation) anti-mouse CD3 and anti-mouse CD28 antibodies overnight at 4 °C. Freshly isolated naive CD4$^+$ T cells (0.5×10^6 cells per ml) were activated with plate-bound antibodies and with mouse IL-2 (3 ng/ml^{-1}) and human TGF-β1 (10 ng/ml^{-1}) for iT_{reg} differentiation, with mouse IL-2 (10 ng/ml^{-1}) and mouse IL-12 (20 ng/ml^{-1}) for T_H1 differentiation, with mouse IL-2 (2 ng/ml^{-1}), mouse IL-4 (50 ng/ml^{-1}) and anti-mouse IFN-γ (10 μg/ml^{-1}) for T_H2 differentiation, or with mouse IL-6 (50 ng/ml^{-1}), human TGF-β1 (20 ng/ml^{-1}), anti-mouse IL-2 (8 μg/ml^{-1}), anti-mouse IL-4 (8 μg/ml^{-1}), and anti-mouse IFN-γ (8 μg/ml^{-1}) for T_H17 differentiation. In some experiments, Vig (1 mM), GABA (0.1 μM–1 mM), NV118 (25 μM), $GABA_A$-R antagonists including bicuculline (Bicl, 5 or 50 μM), picrotoxin (PicroT, 5 or 50 μM) and flumazenil (10 or 1 μM), R162 (20 μM), oligomycin (1.5 μM), FCCP (1 μM), or AG (0.2 mM) was added to cell culture medium. Additional information on cytokines, antibodies and chemicals is listed in Supplementary Table 1.

Flow cytometry

For analysing surface markers, cells were stained in phosphate-buffered saline (PBS) containing 2% (wt/vol) BSA and the appropriate antibodies

from BioLegend. For analysing the intracellular cytokines IFN-γ and IL-17A, T cells were stimulated for 4 hrs with eBioscience™ Cell Stimulation Cocktail (eBioscience) before being stained with cell surface antibodies. Cells were then fixed and permeabilized using FoxP3 Fixation/Permeabilization solution according to the manufacturer's instructions (eBioscience). Cell proliferation was assessed using CFSE staining according to the manufacturer's instructions (Invitrogen). Cell viability was evaluated by 7AAD staining according to the manufacturer's instructions (BioLegend). For analysing DNA/RNA content, cells were collected and stained for surface markers before being fixed with 4% paraformaldehyde for 30 min at 4 °C, followed by a permeabilization step with FoxP3 permeabilization solution (eBioscience). Cells were stained with 7AAD for 5 min and then stained with pyronin-Y (4 μg/ml^{-1}; PE) for 30 min before being analysed using flow cytometer with the PerCP channel for 7AAD (DNA) and PE channel for pyronin-Y (RNA). A protein synthesis assay kit (Item No.601100, Cayman) was used for analysing protein content. Briefly, cells were incubated with *O*-propargyl-puromycin (OPP) for 1 hr and then they were fixed and stained with 5 FAM-azide staining solutions before being analysed using a flow cytometer with the FITC channel. For analysing the cell cycle profile, cells were incubated with 10 μg/ml^{-1} BrdU for 1 hr, followed by cell surface staining, fixation and permeabilization based on the Phase-Flow Alexa Fluor 647 BrdU Kit (BioLegend). Flow cytometry data were acquired on Novocyte (ACEA Biosciences) and were analysed with FlowJo software (TreeStar). Additional information on flow cytometry antibodies is listed in Supplementary Table 2.

T_{reg} cell suppression assay

For the iT_{reg} suppression assay, naive CD4$^+$ T cells isolated from CD45.1 mice using the naive CD4$^+$ mouse T cell isolation kit (BioLegend) were differentiated for 3 d to generate iT_{reg} cells. Naive CD4$^+$ T cells isolated from CD45.2/*Thy1.1* WT donor mice and CD45.2/*Thy1.2 Gabrb3* cKO donor mice were mixed at a 1:1 ratio (as T_{conv} cells) and labelled with CFSE. Then, approximately 5×10^4 T_{conv} cells were mixed with iT_{reg} cells (with indicated ratios) and cultured with 3 ng/ml^{-1} IL-2 and anti-mouse CD3/CD28 beads. Cells were collected 4 d later and processed to assess proliferation by flow cytometry analysis.

Retrovirus production and transduction

Phoenix Eco cells that were cultured in fresh DMEM media (Corning) supplemented with 10% heat-inactivated FBS and 0.5% penicillin-streptomycin were transfected with the control plasmid (pMIC, MSCV-IRES-mCherry) or pMIC-ABAT (Supplementary Table 3). Viral-Boost Reagent (ALSTEM) was added to the culture medium at a 1:600 dilution 6 h after transfection. Cell medium was collected at 48 h after transfection, centrifuged at 300*g* for 10 min, and then filtered through a 0.45-μm filter unit (GVS Filter Technology). Retrovirus Precipitation Solution (ALSTEM) was added to retrovirus-containing supernatant at 1:4 dilution and incubated overnight at 4 °C, followed by centrifugation at 1,500*g* for 30 min at 4 °C to concentrate the virus. Then, approximately 0.3×10^6 activated CD4$^+$ T cells (1 d after activation) were resuspended in 1 ml of retroviral supernatant containing 8 μl/ml^{-1} Lipofectamine (Invitrogen) and cultured under iT_{reg} differentiation for 4 d.

Adoptive cell transfer assays

For homeostatic proliferation in lymphopenic *Rag*$^{-/-}$ mice, naive CD4$^+$ T cells isolated from donor mice using a naive CD4$^+$ mouse T cell isolation kit (BioLegend) were labelled with CFSE. Approximately 1×10^7 cells (mix of WT and KO cells at a 1:1 ratio) in 150 μl of PBS were transferred via caudal venous injection into 6- to 8-week-old sex-matched host mice. Mice were killed between 4–7 d after cell transfer. Lymph nodes and spleen were collected and processed to assess cell ratio and proliferation by flow cytometry analysis.

For antigen-driven proliferation using OT-II mice, naive CD4$^+$ T cells isolated from OT-II/CD45.2 TCR-transgenic donor mice using the naive CD4$^+$ mouse T cell isolation kit (BioLegend) were labelled with CFSE. Approximately 1×10^7 cells (mix of WT and KO cells at a 1:1 ratio) in 150 μl of PBS were transferred via caudal venous injection into 6- to 8-week-old sex-matched CD45.1 host mice. Host mice were immunized subcutaneously in the hock area (50 μl each site) in both legs with 1 mg/ml^{-1} ovalbumin (OVA)$^{323–339}$ peptide (InvivoGen) emulsified with complete Freund adjuvant (CFA; InvivoGen). The mice were then killed 8 d after immunization. Lymph nodes were collected and processed to assess cell ratio, proliferation and protein expression by flow cytometry analysis.

EAE

Mice were immunized subcutaneously with 100 μg of myelin oligodendrocyte glycoprotein $(MOG)_{35–55}$ peptide emulsified in CFA, which was made from IFA (Difco) plus *Mycobacterium tuberculosis* (Difco). Mice were injected intraperitoneally with 200 ng of pertussis toxin (PTX, List Biological Laboratories) on the day of immunization and 2 d later. In the experiments shown in Fig. 4j,k and Extended Data Fig. 5c,d, the mice were injected intraperitoneally with 250 mg/kg^{-1} of Vig in 100 μl PBS daily from day 3 after immunization throughout the end of the experiment. In the experiments shown in Fig. 5g,h and Extended Data Fig. 9c,d, the animals were injected with PTX only once on the day of immunization for a suboptimal EAE induction. All mice were observed daily for clinical signs and scored as described previously[10]. In some experiments, the mice were killed when the control mice reached the onset of symptoms. The CNS (brain and spinal cord), spleen and peripheral lymph nodes were collected and mashed to generate the single-cell suspension. The cell suspension was centrifuged on a 30%/70% Percoll gradient at 500*g* for 30 min to isolate mononuclear cells from the CNS, followed by cell surface and intracellular staining and flow cytometry analysis described above.

Stable isotope labelling experiments

[$^{13}C_5$]Gln, [$^{13}C_6$]Arg and [$^{13}C_6$]Glc labelling of T_H17 cells. Naive CD4$^+$ T cells isolated from WT mice were polarized for 72 h under T_H17 culture conditions before being collected and reseeded at 2×10^6 cells per ml in a conditional medium (RPMI-1640) containing 4 mM [$^{13}C_5$]Gln, 1 mM [$^{13}C_6$]Arg or 10 mM [$^{13}C_6$]Glc. After 12 h of culture, around 1×10^7 cells for each sample were collected and washed three times with PBS before being snap-frozen.

[$^{13}C_6$]Arg labelling of T_H17 cells. T_H17 cells (as described above) were pretreated with vehicle or Vig (1 mM) for 1 h before being collected and reseeded at a density of 2×10^6 cells per ml in a conditional medium (RPMI-1640) containing 4 mM 1 mM [$^{13}C_6$]Arg with vehicle or Vig (1 mM). After 6 h of culture, around 1×10^7 cells for each sample were collected and washed three times with PBS before being snap-frozen.

[$^{13}C_4$]Put labelling of T_H17 cells. T_H17 cells (as described above) were pretreated with vehicle, Vig (1 mM), or AG (0.2 mM) for 1 h and then collected and reseeded at a density of 2×10^6 cells per ml in a conditional medium (RPMI-1640) containing 0.1 mM [$^{13}C_4$]Put and 10 μM Arg and with vehicle, Vig (1 mM), or AG (0.2 mM) treatment. After 6 h of culture, around 1×10^7 cells for each sample were collected and washed three times with PBS before being snap-frozen.

[$^{13}C_4$]GABA labelling of T_H17, iT_{reg} and T_H1 cells. Naive CD4$^+$ T cells isolated from WT mice were polarized for 72 h under T_H17, iT_{reg} or T_H1 culture conditions before being collected and re-seeded at a density of 2×10^6 cells per ml in a conditional medium (RPMI-1640) containing 0.5 mM [$^{13}C_4$]GABA, 0.1 mM Gln and the $GABA_A$-R antagonist bicuculline (5 μM). After 12 h of culture, around 1×10^7 cells for each sample were collected and washed three times with PBS before being snap-frozen.

[$^{13}C_4$]GABA labelling of T_H17 cells with Vig. T_H17 cells (as described above) generated from WT or *Abat* cKO mice were pretreated with vehicle or Vig (1 mM) for 1 h before being collected and reseeded at a density of 2×10^6 cells per ml in the conditional medium containing 0.5 mM [$^{13}C_4$]GABA, 0.1 mM Gln and the $GABA_A$-R antagonist bicuculline (5 μM) and with vehicle or Vig (1 mM) treatment. After 12 h of culture, around 1×10^7 cells for each sample were collected and washed three times with PBS before being snap-frozen.

[$^{13}C_5$]Gln labelling of T_H17 cells with multiple inhibitors. T_H17 cells (as described above) were pretreated with vehicle, Vig (1 mM) or R162 (20 μM) for 1 h and then collected and reseeded at a density of 2×10^6 cells per ml in a conditional medium (RPMI-1640) containing 4 mM [$^{13}C_5$]Gln and with vehicle, Vig (1 mM), R162 (20 μM) or the combination of Vig and R162 treatment. After 6 h of culture, around 1×10^7 cells for each sample were collected and washed three times with PBS before being snap-frozen. Additional information on stable isotope labelling is listed in Supplementary Table 4.

Gas chromatography–mass spectrometry sample preparation and analysis

GC–MS was performed as previously described[57], and cell pellets were resuspended in 0.45 ml of −20 °C methanol/water (1:1 v/v) containing 20 μM L-norvaline as internal standard. Further extraction was performed by adding 0.225 ml of chloroform followed by vortexing and centrifugation at 15,000*g* for 5 min at 4 °C. The upper aqueous phase was evaporated under vacuum using a Speedvac centrifugal evaporator. Separate tubes containing varying amounts of standards were evaporated. Dried samples and standards were dissolved in 30 μl of 20 mg/ml^{-1} isobutylhydroxylamine hydrochloride (TCI #I0387) in pyridine and incubated for 20 min at 80 °C. An equal volume of *N*-tert-butyldimethylsilyl-*N*-methyltrifluoroacetamide (MTBSTFA) (Soltec Ventures) was added and incubated for 60 min at 80 °C. After derivatization, samples and standards were analysed by GC–MS using an Rxi-5ms column (15 m × 0.25 internal diameter × 0.25 μm, Restek) installed in a Shimadzu QP-2010 Plus GC–MS instrument. GC–MS was programmed with an injection temperature of 250 °C, injection volume of 1.0 μl and a split ratio of 1/10. The GC oven temperature was initially 130 °C for 4 min, rising to 250 °C at 6 °C min^{-1} and to 280 °C at 60 °C min^{-1} with a final hold at this temperature for 2 min. GC flow rate, with helium as the carrier gas, was 50 cm s^{-1}. GC–MS interface temperature was 300 °C, and the (electron impact) ion source temperature was 200 °C, with an ionization voltage of 70 eV. Fractional labelling from ^{13}C-labelled substrates and mass isotopomer distributions were calculated as described previously[57]. Data from standards were used to construct standard curves in MetaQuant[58], from which metabolite amounts in samples were calculated. Metabolite amounts were corrected for the recovery of the internal standard and for ^{13}C labelling to yield total (labelled and unlabelled) quantities in nanomoles per sample and then adjusted by cell number.

Liquid chromatography–mass spectrometry sample preparation and analysis

Naive $CD4^+$ T cells were polarized under T_H0, T_H1, T_H17 and iT_{reg} culture conditions or cultured with IL-7 (T_{nai} condition) for 72 h. Then, the cells were collected, washed with PBS and reseeded at a density of 5×10^6 cells per ml in fresh medium. After 6 h of culture, the cell medium was collected and snap-frozen. Sample preparation and analysis were carried out as described previously at Metabolon[59]. In brief, sample preparation involved protein precipitation and removal with methanol, shaking and centrifugation. The resulting extracts were profiled on an accurate mass global metabolomics platform consisting of multiple arms differing by chromatography methods and MS ionization modes to achieve broad coverage of compounds differing by physiochemical properties such as mass, charge, chromatography separation and ionization behaviour. Metabolites were identified by automated comparison of the ion features in the experimental samples to a reference library of chemical standard entries that included retention time, molecular weight (*m/z*), preferred adducts and in-source fragments as well as associated MS spectra and were curated by visual inspection for quality control using a software developed at Metabolon.

Metabolite quantification

In some experiments, T_H17 cells were suspended at a density of 5×10^6 cells per ml with medium containing vehicle or Vig (1 mM). After 6 h of culture, blank medium (without cells) and spent medium were collected. The levels of Gln and Glu were measured using the Bioanalyzer (YSI 2900). Following the manufacturer's instructions, Arg and GAB quantities were determined by L-Arginine Assay Kit (BioVision) and GABA Research ELISA Kit (LDN). Consumption or production of each metabolite was determined by calculating the difference between blank and spent media.

OCR

Following the manufacturer's instructions, the OCR was determined using the Seahorse XFe96 Analyzer (Agilent Technologies). Briefly, approximately 1×10^5 T_H17 cells were suspended in a 50 μl assay medium (Seahorse XF RPMI Assay Medium, pH 7.4, Agilent Technologies) containing 10 mM Glc, 2 mM Glu and 1 mM pyruvate and were seeded in an XF96 Cell Culture Microplates (Seahorse, Agilent Technologies) precoated with poly(D-lysine) (50 μg ml^{-1}; Millipore). The cells were centrifuged at 200*g* for 2 min on a zero-braking setting to immobilize the cells before they were supplied with an additional 130 μl of assay medium and kept in a non-CO_2 incubator for 30 min. Data analysis was performed using the Seahorse Wave Software (Seahorse, Agilent Technologies). In some experiments, the $GABA_A$-R antagonist bicuculline (5 μM) was added along with GABA to prevent the activation of $GABA_A$-R. Various compounds were injected into each well sequentially to achieve the following final concentrations: 0.5 mM GABA, 1 mM Vig, 20 μM R162, 1.5 μM oligomycin, and 1 μM FCCP.

Western blot analysis, RNA extraction, qPCR, and RNA-seq and NMR analysis of medium

Details are provided in the Supplementary Information.

Statistical analysis

Statistical analysis was conducted using the GraphPad Prism software (GraphPad Software; v 8.0.1). To determine the statistical significance, different tests including unpaired two-tailed Student's *t*-test, one-way ANOVA with Tukey's multiple-comparisons test and two-way ANOVA with Sidak's multiple-comparisons test were used as indicated in the figure legends. The number of experimental repeats is indicated in the figure legends. R software (v 4.2.1) was used for Metabolon and RNA-seq data analysis. *P* values that were considered significant are shown in the corresponding figures.

Reporting summary

Further information on the research design is available in the Nature Research Reporting Summary linked to this article.

Data availability

The RNA-seq datasets generated for this study can be found in the Gene Expression Omnibus under accession GSE190818. The authors declare that all other data supporting the findings of this study are available within the paper and supplementary information files. Source data are provided with this paper.

References

1. Dang, C. V., Reddy, E. P., Shokat, K. M. & Soucek, L. Drugging the 'undruggable' cancer targets. *Nat. Rev. Cancer* **17**, 502–508 (2017).

2. Barnie, P. A., Lin, X., Liu, Y., Xu, H. & Su, Z. IL-17 producing innate lymphoid cells 3 (ILC3) but not Th17 cells might be the potential danger factor for preeclampsia and other pregnancy associated diseases. *Int J. Clin. Exp. Pathol.* **8**, 11100–11107 (2015).
3. Stine, Z. E., Schug, Z. T., Salvino, J. M. & Dang, C. V. Targeting cancer metabolism in the era of precision oncology. *Nat Rev Drug Discov.* https://doi.org/10.1038/s41573-021-00339-6 (2021).
4. Muir, A. et al. Environmental cystine drives glutamine anaplerosis and sensitizes cancer cells to glutaminase inhibition. *eLife* **6**, https://doi.org/10.7554/eLife.27713 (2017).
5. Sivanand, S. & Vander Heiden, M. G. Emerging roles for branched-chain amino acid metabolism in cancer. *Cancer Cell* **37**, 147–156 (2020).
6. Puleston, D. J., Villa, M. & Pearce, E. L. Ancillary activity: beyond core metabolism in immune cells. *Cell Metab.* **26**, 131–141 (2017).
7. O'Neill, L. A., Kishton, R. J. & Rathmell, J. A guide to immunometabolism for immunologists. *Nat. Rev. Immunol.* **16**, 553–565 (2016).
8. Pinu, F. R. & Villas-Boas, S. G. Extracellular microbial metabolomics: the state of the art. *Metabolites* https://doi.org/10.3390/metabo7030043 (2017).
9. Beale, D. J. et al. Application of metabolomics to understanding biofilms in water distribution systems: a pilot study. *Biofouling* **29**, 283–294 (2013).
10. Wu, R. et al. De novo synthesis and salvage pathway coordinately regulate polyamine homeostasis and determine T cell proliferation and function. *Sci. Adv.* https://doi.org/10.1126/sciadv.abc4275 (2020).
11. Puleston, D. J. et al. Polyamine metabolism is a central determinant of helper T cell lineage fidelity. *Cell* **184**, 4186–4202 (2021).
12. Wagner, A. et al. Metabolic modeling of single Th17 cells reveals regulators of autoimmunity. *Cell* **184**, 4168–4185 (2021).
13. Milo, R. & Phillips, R. *Cell Biology by the Numbers*. (Garland Science, 2015).
14. Bhandage, A. K. & Barragan, A. GABAergic signaling by cells of the immune system: more the rule than the exception. *Cell Mol. Life Sci.* **78**, 5667–5679 (2021).
15. Vigabatrin. *Lancet* **1**, 532-533 (1989).
16. Lippert, B., Metcalf, B. W., Jung, M. J. & Casara, P. 4-Amino-hex-5-enoic acid, a selective catalytic inhibitor of 4-aminobutyric-acid aminotransferase in mammalian brain. *Eur. J. Biochem* **74**, 441–445 (1977).
17. Brady, S. *Basic Neurochemistry: Molecular, Cellular and Medical Aspects* (Elsevier, 2005).
18. Shelp, B. J. et al. Hypothesis/review: contribution of putrescine to 4-aminobutyrate (GABA) production in response to abiotic stress. *Plant Sci.* **193–194**, 130–135 (2012).
19. Seiler, N. & Eichentopf, B. 4-Aminobutyrate in mammalian putrescine catabolism. *Biochem. J.* **152**, 201–210 (1975).
20. Brunengraber, H. & Roe, C. R. Anaplerotic molecules: current and future. *J. Inherit. Metab. Dis.* **29**, 327–331 (2006).
21. Lian, G. et al. Glutathione de novo synthesis but not recycling process coordinates with glutamine catabolism to control redox homeostasis and directs murine T cell differentiation. *eLife* **7**, https://doi.org/10.7554/eLife.36158 (2018).
22. Johnson, M. O. et al. Distinct regulation of Th17 and Th1 cell differentiation by glutaminase-dependent metabolism. *Cell* **175**, 1780–1795 (2018).
23. Jin, L. et al. Glutamate dehydrogenase 1 signals through antioxidant glutathione peroxidase 1 to regulate redox homeostasis and tumor growth. *Cancer Cell* **27**, 257–270 (2015).
24. Ehinger, J. K. et al. Cell-permeable succinate prodrugs bypass mitochondrial complex I deficiency. *Nat. Commun.* **7**, 12317 (2016).
25. Zhou, L., Chong, M. M. & Littman, D. R. Plasticity of CD4$^+$ T cell lineage differentiation. *Immunity* **30**, 646–655 (2009).
26. Chi, H. Regulation and function of mTOR signalling in T cell fate decisions. *Nat. Rev. Immunol.* **12**, 325–338 (2012).
27. Powell, J. D. & Delgoffe, G. M. The mammalian target of rapamycin: linking T cell differentiation, function, and metabolism. *Immunity* **33**, 301–311 (2010).
28. Jerne, N. K. Towards a network theory of the immune system. *Ann. Immunol.* **125C**, 373–389 (1974).
29. Ader, R., Cohen, N. & Felten, D. Psychoneuroimmunology: interactions between the nervous system and the immune system. *Lancet* **345**, 99–103 (1995).
30. Cohen, I. R. *Tending Adam's Garden: Evolving the Cognitive Immune Self* (Elsevier, 2000).
31. Tauber, A. I. *Immunity: The Evolution of an Idea* (Oxford University Press, 2017).
32. Vedhara, K., Irwin, M. R. & Irwin, M. *Human Psychoneuroimmunology* (Oxford University Press on Demand, 2005).
33. Tannahill, G. M. et al. Succinate is an inflammatory signal that induces IL-1β through HIF-1α. *Nature* **496**, 238–242 (2013).
34. Zhang, B. et al. B cell-derived GABA elicits IL-10$^+$ macrophages to limit anti-tumour immunity. *Nature* **599**, 471–476 (2021).
35. Geiger, R. et al. L-Arginine modulates T cell metabolism and enhances survival and anti-tumor activity. *Cell* **167**, 829–842 e813 (2016).
36. Wang, R. et al. The transcription factor Myc controls metabolic reprogramming upon T lymphocyte activation. *Immunity* **35**, 871–882 (2011).
37. Klysz, D. et al. Glutamine-dependent α-ketoglutarate production regulates the balance between T helper 1 cell and regulatory T cell generation. *Sci. Signal.* **8**, ra97 (2015).
38. Palazon, A., Goldrath, A. W., Nizet, V. & Johnson, R. S. HIF transcription factors, inflammation, and immunity. *Immunity* **41**, 518–528 (2014).
39. Raghuraman, S., Donkin, I., Versteyhe, S., Barres, R. & Simar, D. The emerging role of epigenetics in inflammation and immunometabolism. *Trends Endocrinol. Metab.* **27**, 782–795 (2016).
40. Chen, X. et al. Succinate dehydrogenase/complex II is critical for metabolic and epigenetic regulation of T cell proliferation and inflammation. *Sci. Immunol.* **7**, eabm8161 (2022).
41. Birkner, K. et al. β1-Integrin- and Kv1.3 channel-dependent signaling stimulates glutamate release from Th17 cells. *J. Clin. Invest* **130**, 715–732 (2020).
42. Patel, C. H., Leone, R. D., Horton, M. R. & Powell, J. D. Targeting metabolism to regulate immune responses in autoimmunity and cancer. *Nat. Rev. Drug Discov.* **18**, 669–688 (2019).
43. Wang, R. & Green, D. R. Metabolic reprogramming and metabolic dependency in T cells. *Immunol. Rev.* **249**, 14–26 (2012).
44. Lock, C. et al. Gene-microarray analysis of multiple sclerosis lesions yields new targets validated in autoimmune encephalomyelitis. *Nat. Med.* **8**, 500–508 (2002).
45. Han, M. H. et al. Proteomic analysis of active multiple sclerosis lesions reveals therapeutic targets. *Nature* **451**, 1076–1081 (2008).
46. Maas, K. et al. Cutting edge: molecular portrait of human autoimmune disease. *J. Immunol.* **169**, 5–9 (2002).
47. Jin, Z., Mendu, S. K. & Birnir, B. GABA is an effective immunomodulatory molecule. *Amino Acids* **45**, 87–94 (2013).
48. Bhattacharyya, P. K., Phillips, M. D., Stone, L. A., Bermel, R. A. & Lowe, M. J. Sensorimotor cortex γ-aminobutyric acid concentration correlates with impaired performance in patients with MS. *AJNR Am. J. Neuroradiol.* **34**, 1733–1739 (2013).

49. Cao, G. et al. Reduced GABA levels correlate with cognitive impairment in patients with relapsing-remitting multiple sclerosis. *Eur. Radiol.* **28**, 1140–1148 (2018).
50. Puniya, B. L. et al. Integrative computational approach identifies drug targets in CD4$^+$ T-cell-mediated immune disorders. *NPJ Syst. Biol. Appl.* **7**, 4 (2021).
51. Tian, J., Yong, J., Dang, H. & Kaufman, D. L. Oral GABA treatment downregulates inflammatory responses in a mouse model of rheumatoid arthritis. *Autoimmunity* **44**, 465–470 (2011).
52. Soltani, N. et al. GABA exerts protective and regenerative effects on islet beta cells and reverses diabetes. *Proc. Natl Acad. Sci. USA* **108**, 11692–11697 (2011).
53. Bhat, R. et al. Inhibitory role for GABA in autoimmune inflammation. *Proc. Natl Acad. Sci. USA* **107**, 2580–2585 (2010).
54. Carmans, S. et al. Systemic treatment with the inhibitory neurotransmitter γ-aminobutyric acid aggravates experimental autoimmune encephalomyelitis by affecting proinflammatory immune responses. *J. Neuroimmunol.* **255**, 45–53 (2013).
55. Tian, J., Dang, H., Wallner, M., Olsen, R. & Kaufman, D. L. Homotaurine, a safe blood-brain barrier permeable GABAA-R-specific agonist, ameliorates disease in mouse models of multiple sclerosis. *Sci. Rep.* **8**, 16555 (2018).
56. Skarnes, W. C. et al. A conditional knockout resource for the genome-wide study of mouse gene function. *Nature* **474**, 337–342 (2011).
57. Ratnikov, B. et al. Glutamate and asparagine cataplerosis underlie glutamine addiction in melanoma. *Oncotarget* **6**, 7379–7389 (2015).
58. Bunk, B. et al. MetaQuant: a tool for the automatic quantification of GC/MS-based metabolome data. *Bioinformatics* **22**, 2962–2965 (2006).
59. Evans, A. M., DeHaven, C. D., Barrett, T., Mitchell, M. & Milgram, E. Integrated, nontargeted ultrahigh performance liquid chromatography/electrospray ionization tandem mass spectrometry platform for the identification and relative quantification of the small-molecule complement of biological systems. *Anal. Chem.* **81**, 6656–6667 (2009).

Acknowledgements

This work was supported by 1U01CA232488-01 from the National Institute of Health (Cancer Moonshot program), 2R01AI114581-06 and R01CA247941 from the National Institutes of Health, V2014-001 from the V-Foundation and 128436-RSG-15-180-01-LIB from the American Cancer Society (to R.W.) and by T32 Ruth L. Kirschstein National Research Service Award CA 269052 from the National Institutes of Health (to S.K.). The Sanford Burnham Prebys Cancer Metabolism Core was supported by the SBP NVI Cancer Center Support Grant P30 CA030199 (to D.A.S.). The Center for Environmental and Systems Biochemistry Core was supported in part by the Markey Cancer Center support grant P30CA177558 (to A.N.L.).

Author contributions

R.W. conceptualized the study, designed all experiments and directed the study. R.W. and S.K. wrote the manuscript with input from all authors. S.K., P.L. and D.A.S. performed the experiments and analysed the data. S.K. performed in vitro cell-related experiments such as mouse cell isolation, cell culture, ELISA, flow cytometry, western blotting, qPCR, LC–MS Metabolon and GC–MS ^{13}C tracer samples collection, and in vivo mouse experiments including inn the EAE and adoptive transfer models. P.L. performed the NMR medium analysis experiment. T.W. and D.A.S. performed sample preparation, the experiment and data analysis for the GC–MS ^{13}C tracer experiment. L.L. performed the ABAT plasmid sequencing, generated all mouse strains and provided mice for all the experiments. M.C. performed the R analysis. T.W.-M.F., H.-J.J.W. and A.N.L. contributed with conceptual design, interpretation of the data and critical review of the manuscript. R.W. obtained the funding and provided supervision. S.K., D.A.S. and A.N.L. contributed with funding. All authors critically reviewed and discussed the results and contributed to and agreed to the final manuscript.

Competing interests

The authors declare no competing interests.

Additional information

Extended data is available for this paper at https://doi.org/10.1038/s42255-022-00638-1.

Supplementary information The online version contains supplementary material available at https://doi.org/10.1038/s42255-022-00638-1.

Correspondence and requests for materials should be addressed to Ruoning Wang.

Peer review information *Nature Metabolism* thanks Qi-Jing Li and the other, anonymous, reviewer(s) for their contribution to the peer review of this work. Primary Handling Editor: Ashley Castellanos-Jankiewicz, in collaboration with the *Nature Metabolism* team.

Reprints and permissions information is available at www.nature.com/reprints.

Publisher's note Springer Nature remains neutral with regard to jurisdictional claims in published maps and institutional affiliations.

https://doi.org/10.1038/s42255-022-00638-1

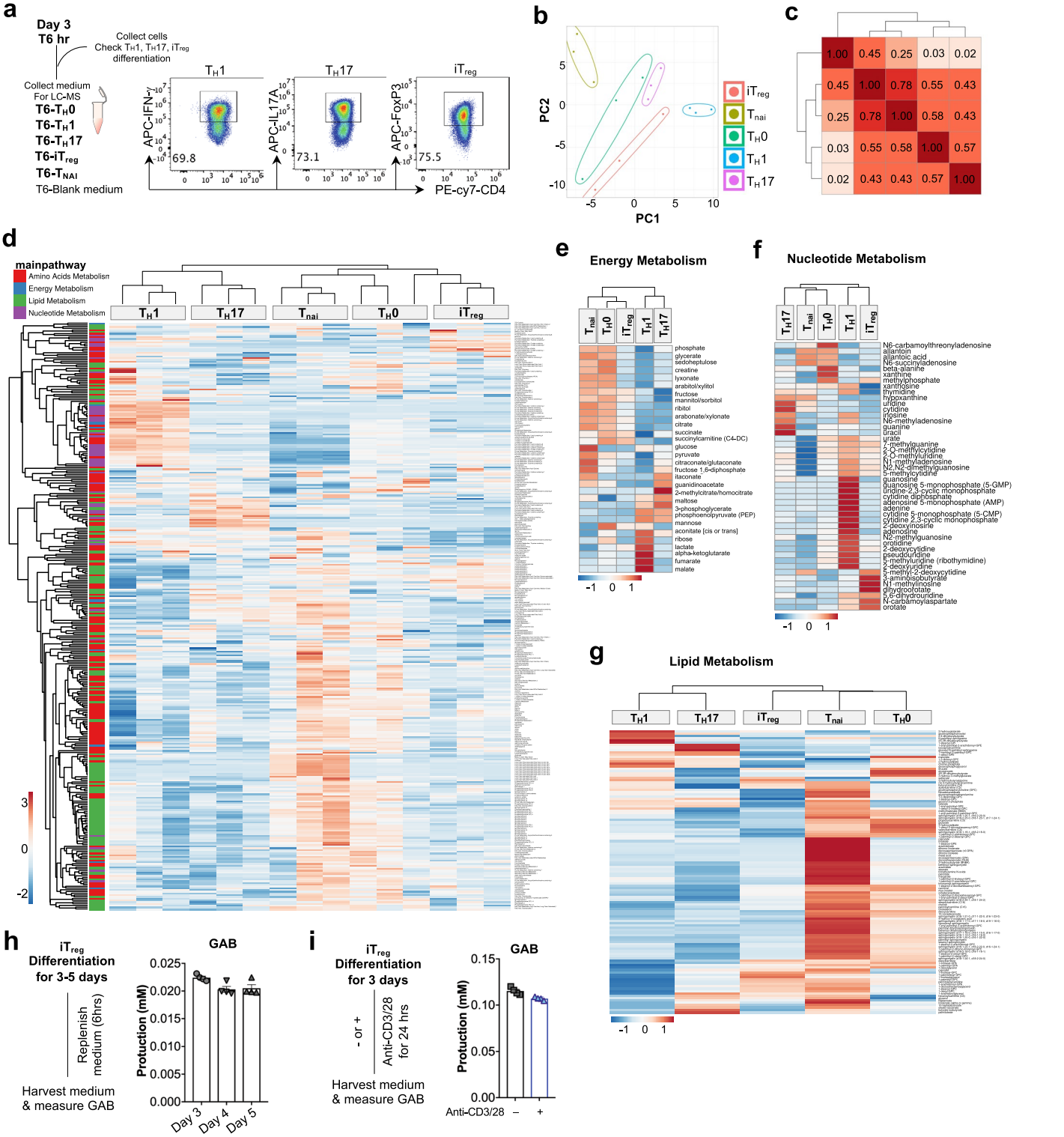

Extended Data Fig. 1 | Distinctive extracellular metabolome profiles characterize T cell subsets. a, Cytokine production of indicating T cell subsets was determined by flow cytometer. **b**, Principal component analysis (PCA) for the correlations among each subset. **c**, Pairwise comparison of the statistical analysis, the numbers reflect the correlation R values. **d**, Extracellular metabolites in indicated T cell subsets were profiled by LC-MS. The hierarchical clustering heatmap represents the value of the relative amount (see color scale). **e-g**, Extracellular metabolites associated with energy metabolism (**e**), nucleotide metabolism (**f**), and lipid metabolism (**g**) in indicated T cell subsets were profiled by LC-MS. The value for each metabolite represents the average of triplicates. The complete metabolomic profile is provided in ***Source Data file 5***. Statistical analysis was performed by R Programming Language (**b**–**g**). **h, i**, As illustrated by the experimental scheme (left), GAB production of iTreg cells in indicated conditions was quantified by a GAB bioassay kit ($n = 4$ biologically independent samples).

https://doi.org/10.1038/s42255-022-00638-1

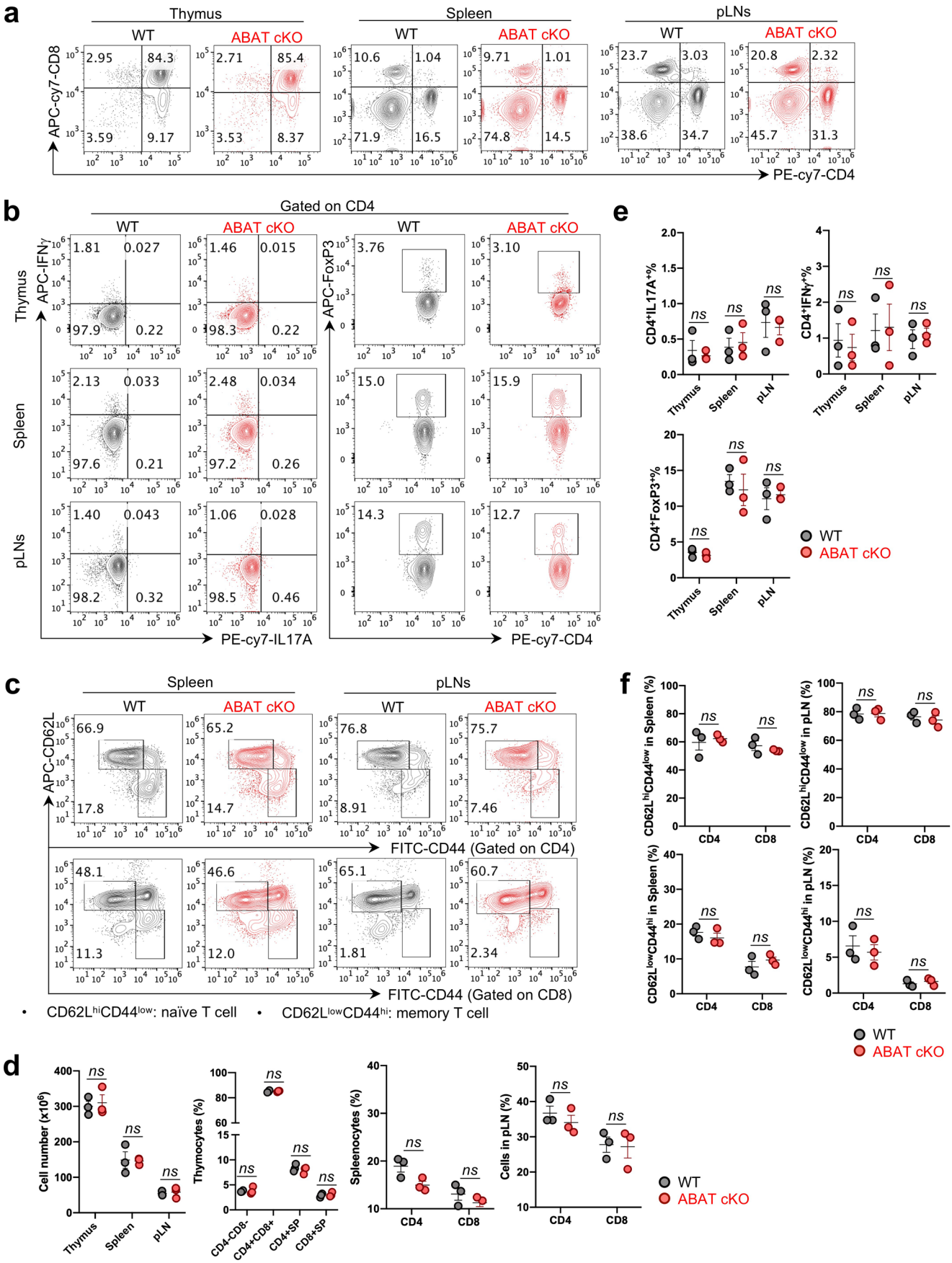

Extended Data Fig. 2 | ABAT is dispensable for normal T cell development after the double-positive stage. a–f, Distribution of CD4$^+$ and CD8$^+$ T cell (**a, d**), indicated intracellular proteins (**b, e**) and surface markers (**c, f**) were determined by flow cytometer. Data are shown as mean ± SEM, $n = 3$ biologically independent samples, significance was calculated by unpaired Two-tail Student's t-test. *ns*, no significant differences.

https://doi.org/10.1038/s42255-022-00638-1

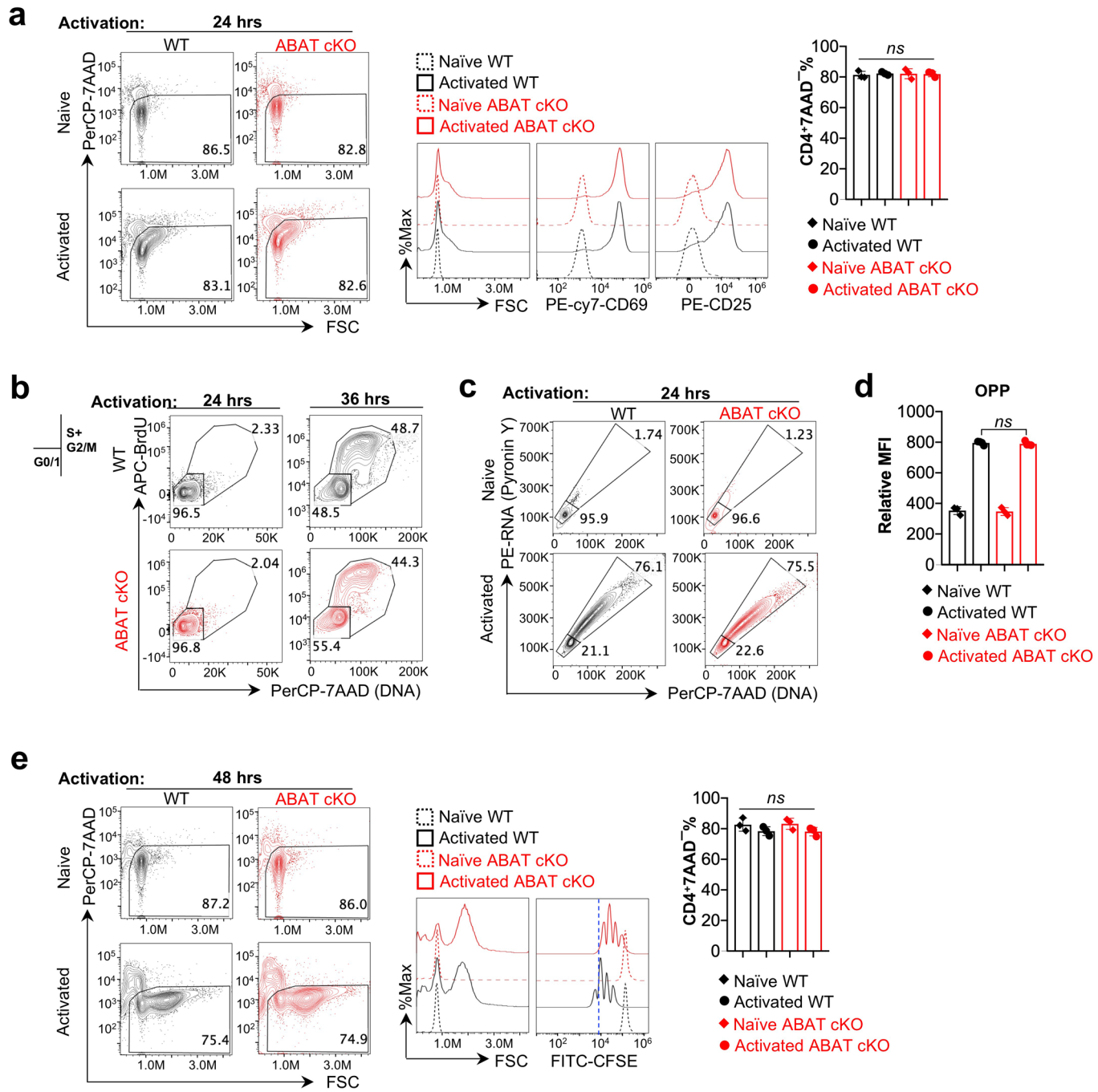

Extended Data Fig. 3 | ABAT is dispensable for T cell activation. a, Cell viability, size and activation markers (**a**), cell cycle profile (**b**), DNA/RNA contents (**c**), protein synthesis activity (**d**), and CFSE dilution and cell viability (**e**) were determined by flow cytometry. Data are shown as mean ± SEM, $n = 3$ biologically independent samples, significance was calculated by Two-way ANOVA with Sidak's multiple comparisons test. *ns*, no significant differences. OPP: o-propargyl-puromycin, MFI: median fluorescence intensity.

https://doi.org/10.1038/s42255-022-00638-1

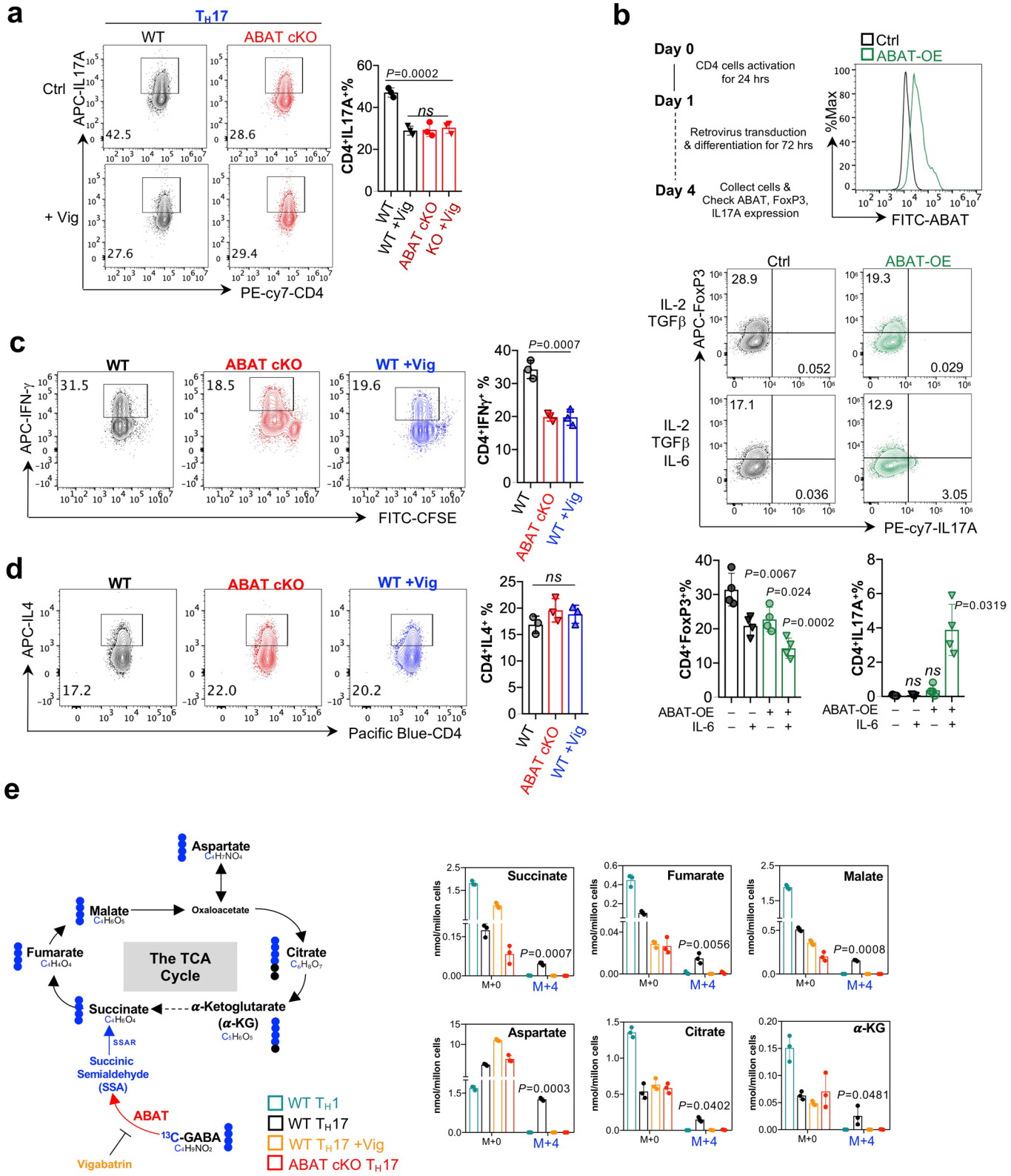

Extended Data Fig. 4 | ABAT regulates T cell differentiation *in vitro*. **a**–**d**, Expression of indicated cytokines in indicated groups was determined by flow cytometry: **a, c, d**, data represents of $n = 3$ biologically independent samples, significance was calculated by one-way ANOVA with Tukey's multiple comparisons test. *ns*, no significant differences. **b**, data represents of $n = 4$ biologically independent samples, unpaired Two-tail Student's t-test. ns, no significant differences. **e**, Diagram of converting [$^{13}C_4$]-GABA (left) to downstream metabolites. Indicated metabolites were quantified by GC-MS ($n = 3$ biologically independent samples). Black dot: ^{12}C; Blue dot: ^{13}C derived from the indicated tracers. Numbers in the X-axis represent those of ^{13}C atoms in given metabolites. Significance was calculated by unpaired Two-tail Student's t-test. ABAT-OE: ABAT overexpression, α-KG: α-Ketoglutarate, M: mass spectrum.

https://doi.org/10.1038/s42255-022-00638-1

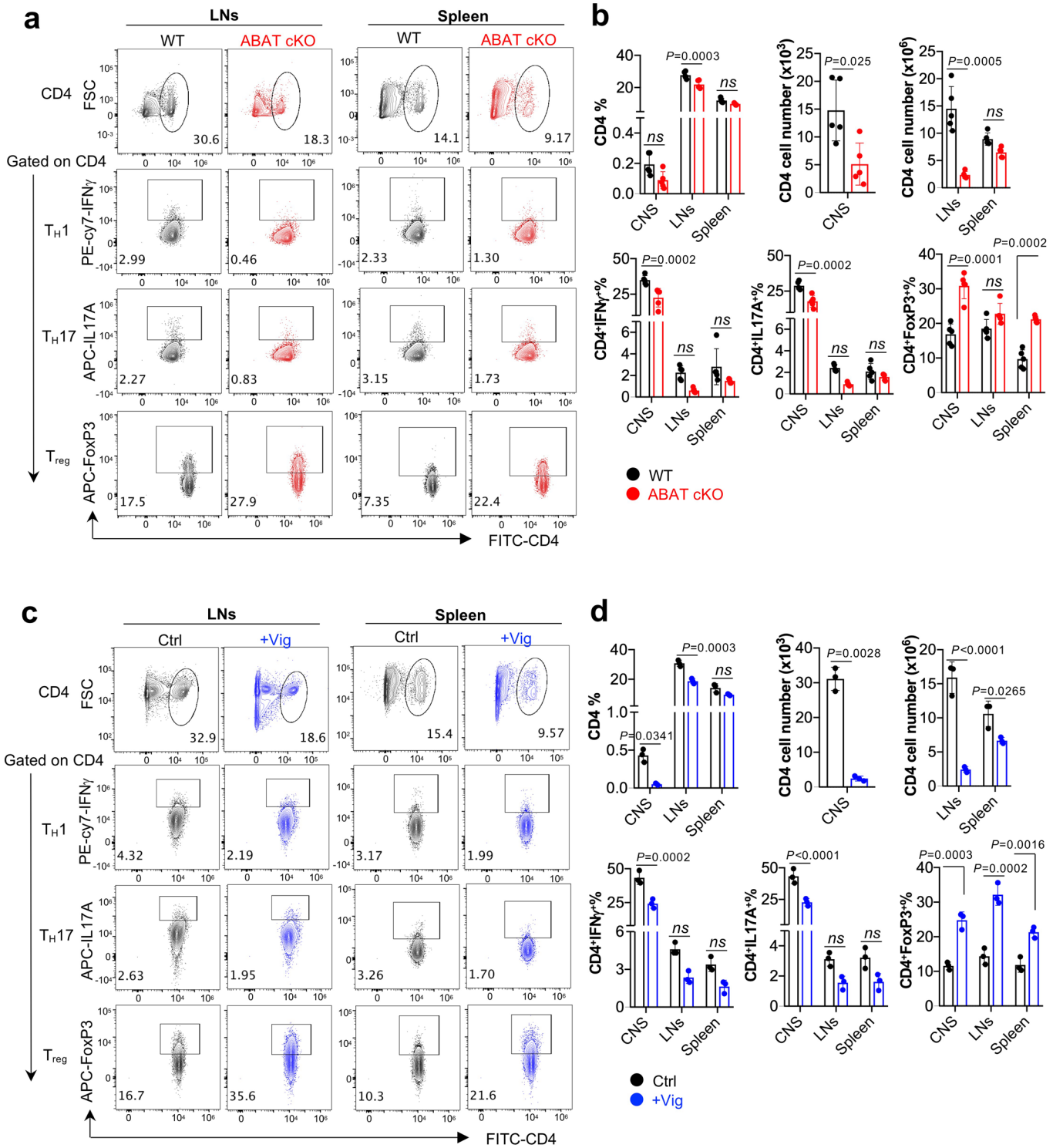

Extended Data Fig. 5 | Genetic ablation or pharmacological inhibition of ABAT reduces T cell inflammation in EAE. a–d, T cells were isolated from indicated sites in experimental animals described in Fig. 4h (**a, b**) and Fig. 4j (**c, d**). The expression of indicated proteins was determined by flow cytometry. Statistical analysis ($n = 3$ biologically independent samples) was calculated by unpaired Two-tail Student's t-test. Data are shown as mean ± SEM, *ns*, no significant differences. Vig: vigabatrin, EAE: experimental autoimmune encephalomyelitis, CNS: central nervous system, LNs: lymph nodes.

https://doi.org/10.1038/s42255-022-00638-1

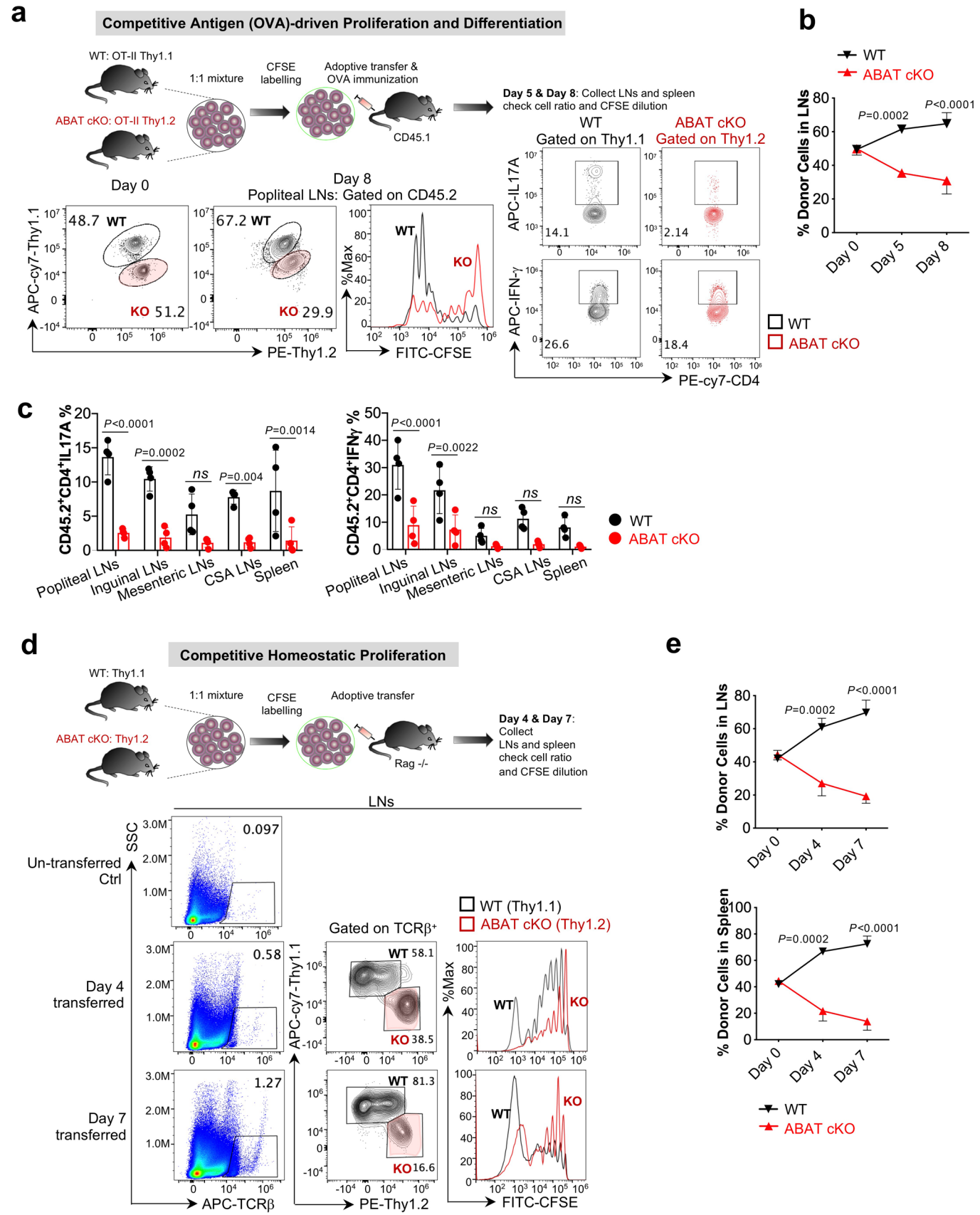

Extended Data Fig. 6 | See next page for caption.

https://doi.org/10.1038/s42255-022-00638-1

Extended Data Fig. 6 | Inhibition of ABAT suppresses T cell proliferation and differentiation *in vivo*. **a**–**c**, As illustrated by the experimental diagram of competitive antigen (OVA)-specific proliferation (**a**, top), the donor cell ratio (**a**, bottom and **b**), CFSE dilution (**a**, bottom), and indicated protein levels (**a**, bottom and **c**), were determined by flow cytometry ($n = 3$ biologically independent samples). **b**, **c**, Data are shown as mean ± SEM, significance was calculated by unpaired Two-tail Student's t-test. *ns*, no significant differences. **d**–**e**, As illustrated by the experimental diagram of competitive homeostatic proliferation (**d**, top). The donor cell ratio (**d**, bottom, and **e**) and CFSE dilution (**d**, bottom) were determined by flow cytometry ($n = 3$ biologically independent samples). **e**, Significance was calculated by unpaired Two-tail Student's t-test. CSA: cervical, submandibular and axilla.

https://doi.org/10.1038/s42255-022-00638-1

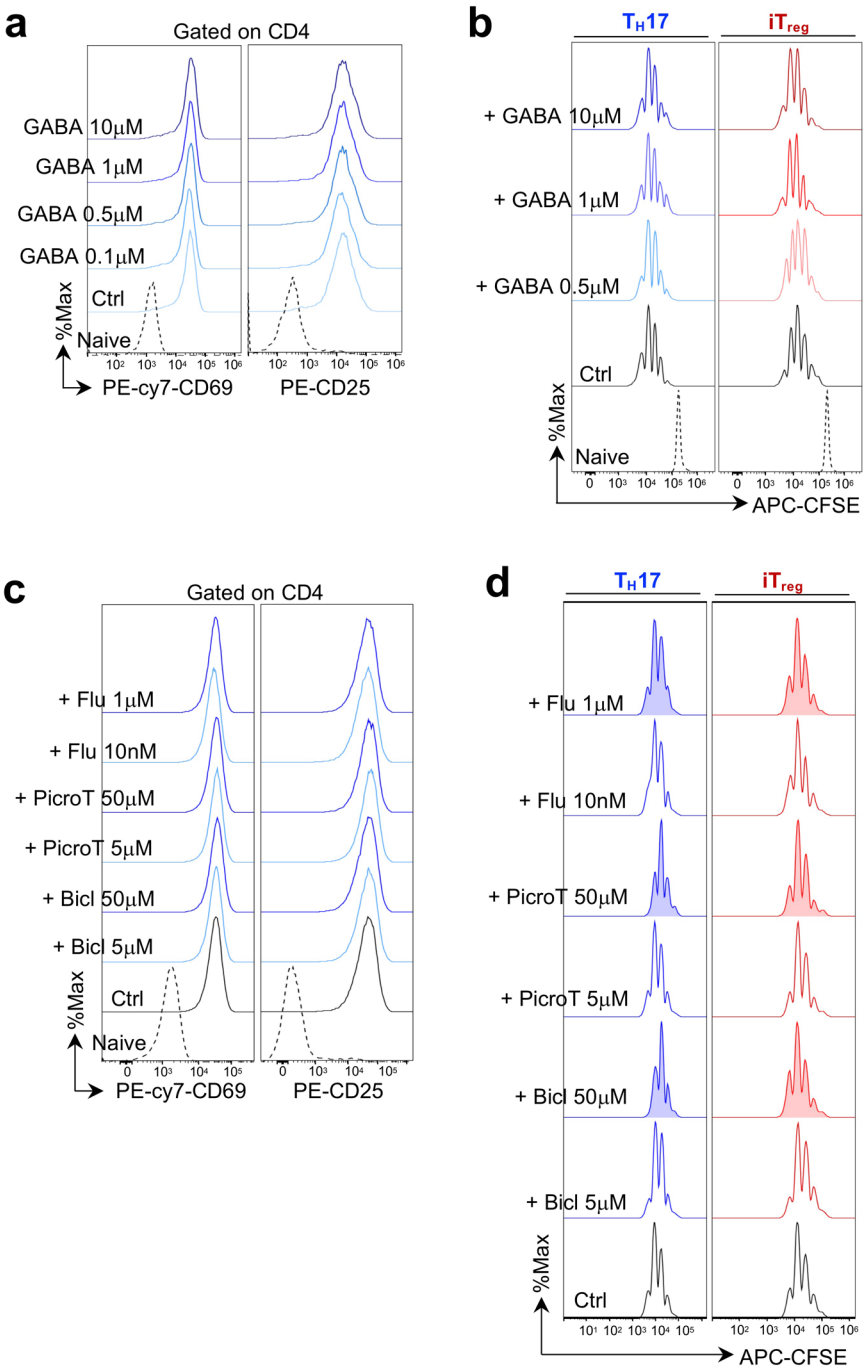

Extended Data Fig. 7 | Modulating GABA receptor-mediated response does not affect activation and proliferation significantly during T_H17 and iT_{reg} differentiation. a–d, Cell activation markers (**a, c**), and CFSE dilution (**b, d**) were determined by flow cytometry ($n = 3$ biologically independent experiments). Bicl: bicuculline, PicroT: picrotoxin, Flu: flumazenil.

https://doi.org/10.1038/s42255-022-00638-1

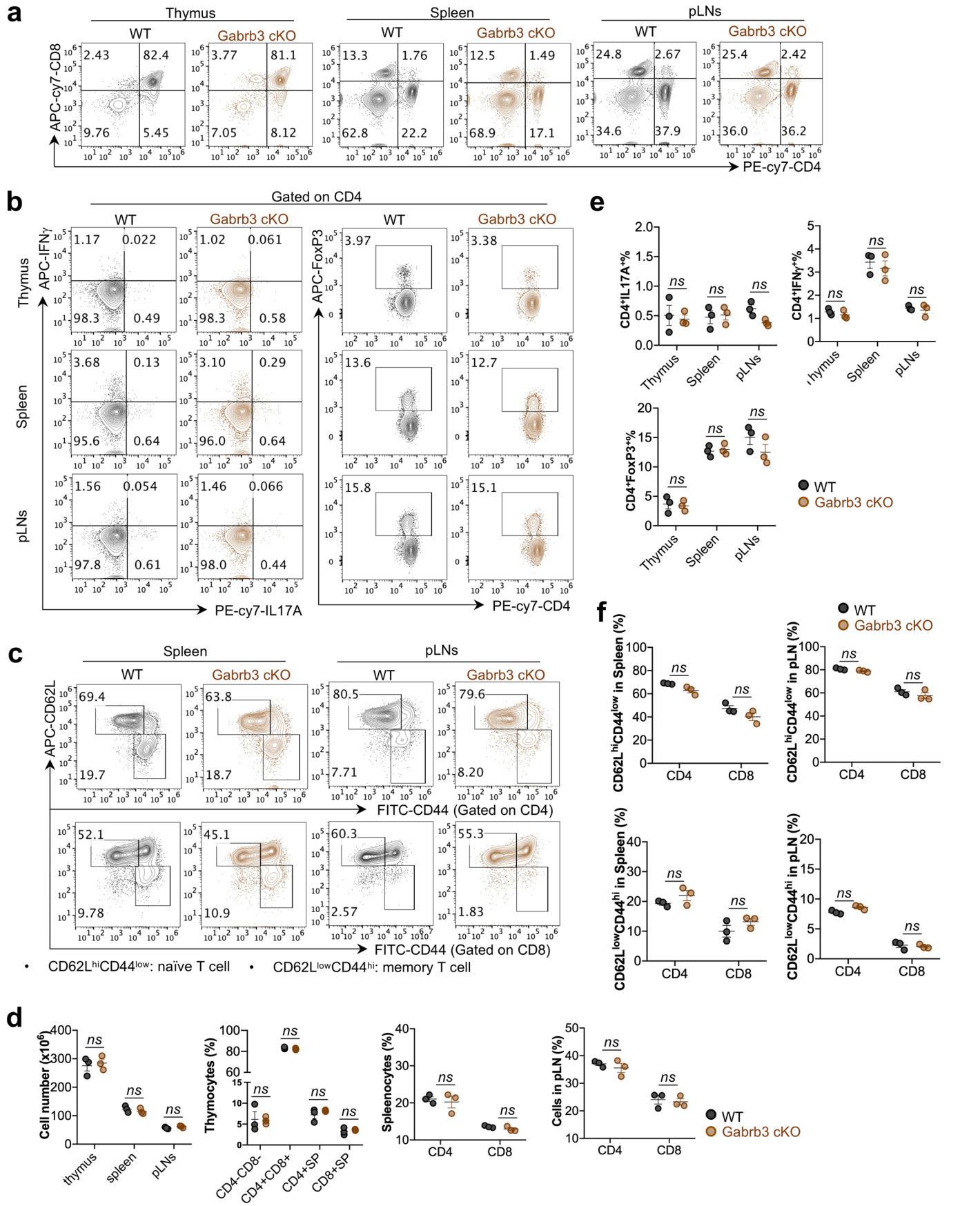

Extended Data Fig. 8 | GABA receptor is dispensable for normal T cell development after the double-positive stage. a–f, Distribution of $CD4^+$ and $CD8^+$ T cell (**a, d**), indicated intracellular proteins (**b, e**), and surface markers (**c, f**) were determined by flow cytometer. Data are shown as mean ± SEM, $n = 3$ biologically independent samples, significance was calculated by unpaired Two-tail Student's t-test. *ns*, no significant differences.

https://doi.org/10.1038/s42255-022-00638-1

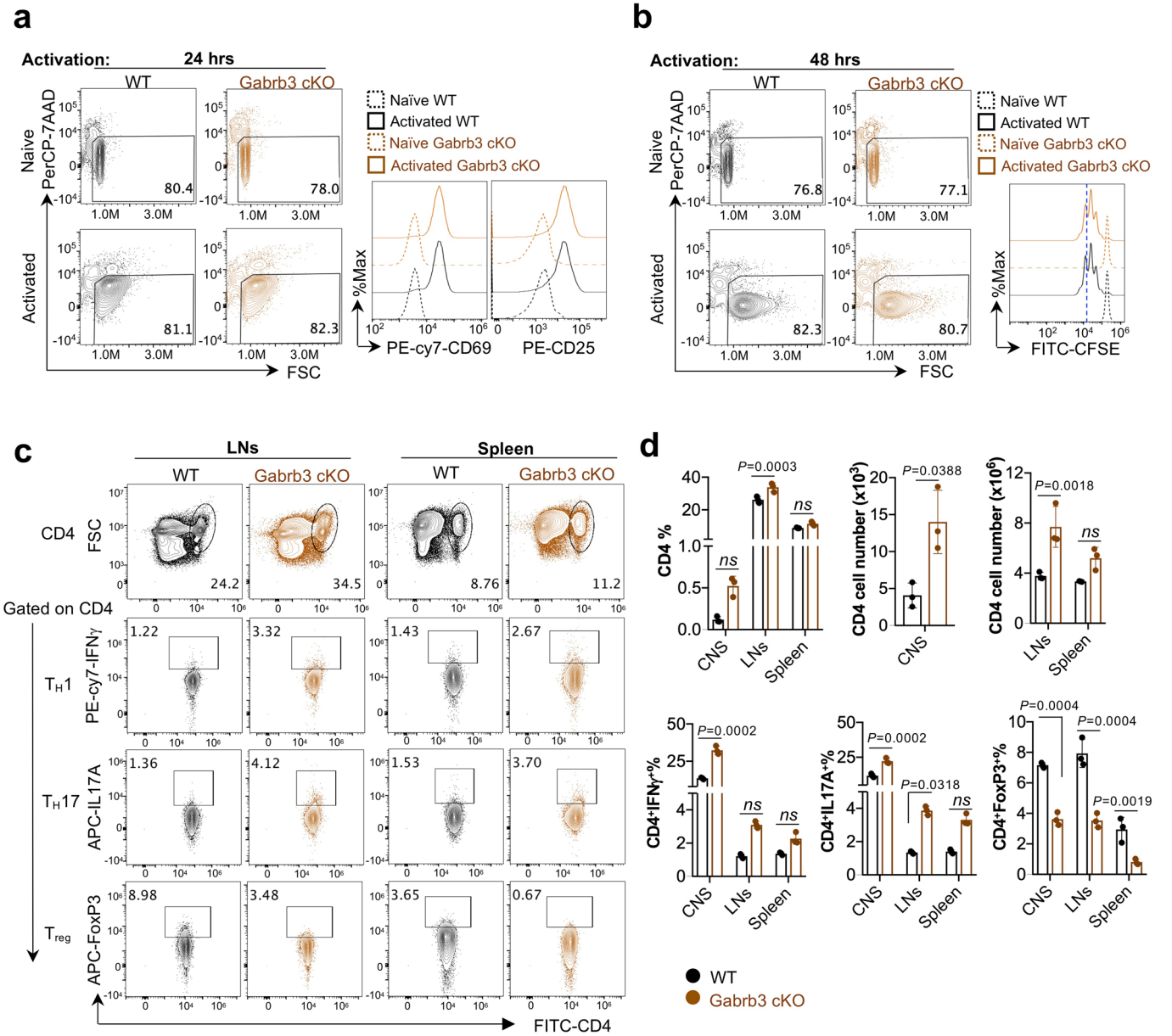

Extended Data Fig. 9 | GABA receptor is required for T cell differentiation but not activation. a, b, Cell viability, cell activation markers (**a**), and CFSE dilution (**b**) were determined by flow cytometry ($n = 3$ biologically independent experiments). **c**, T cells were isolated from indicated sites in experimental animals described **in** Fig. 5g. The expression of indicated proteins was determined by flow cytometry. **d**, Statistical analysis ($n = 3$ biologically independent samples) was calculated by unpaired Two-tail Student's t-test. Data are shown as mean ± SEM, *ns*, no significant differences. EAE: experimental autoimmune encephalomyelitis, CNS: central nervous system, LNs: lymph nodes.

https://doi.org/10.1038/s42255-022-00638-1

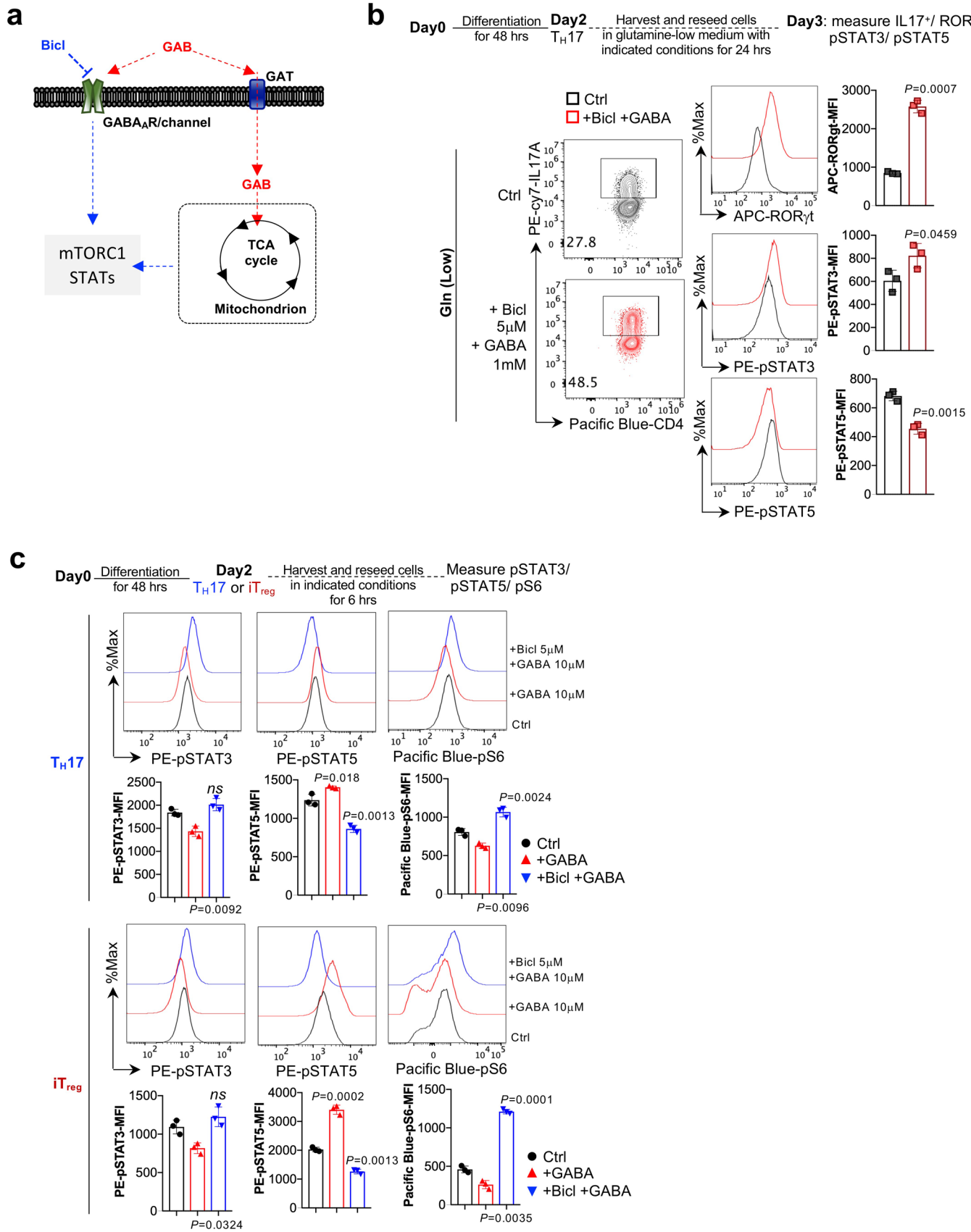

Extended Data Fig. 10 | GAB controls T cell signaling pathways through both receptor and mitochondrial metabolism. a, Schematic diagram of GAB metabolism and GABAA-R-mediated signaling response. **b, c**, The schematic diagram of the experiment (top), the expression of indicated proteins from each group was determined by flow cytometry ($n = 3$ biologically independent samples). Data are shown as mean ± SEM. **b**, Significance was calculated by unpaired Two-tail Student's t-test. **c**, Significance was calculated by one-way ANOVA with Tukey's multiple comparisons test. *ns*, no significant differences.

nature portfolio

Corresponding author(s): Ruoning Wang

Last updated by author(s): 2022/08/03

Reporting Summary

Nature Portfolio wishes to improve the reproducibility of the work that we publish. This form provides structure for consistency and transparency in reporting. For further information on Nature Portfolio policies, see our Editorial Policies and the Editorial Policy Checklist.

Statistics

For all statistical analyses, confirm that the following items are present in the figure legend, table legend, main text, or Methods section.

n/a	Confirmed	
☐	☒	The exact sample size (*n*) for each experimental group/condition, given as a discrete number and unit of measurement
☐	☒	A statement on whether measurements were taken from distinct samples or whether the same sample was measured repeatedly
☐	☒	The statistical test(s) used AND whether they are one- or two-sided *Only common tests should be described solely by name; describe more complex techniques in the Methods section.*
☒	☐	A description of all covariates tested
☒	☐	A description of any assumptions or corrections, such as tests of normality and adjustment for multiple comparisons
☐	☒	A full description of the statistical parameters including central tendency (e.g. means) or other basic estimates (e.g. regression coefficient) AND variation (e.g. standard deviation) or associated estimates of uncertainty (e.g. confidence intervals)
☐	☒	For null hypothesis testing, the test statistic (e.g. *F*, *t*, *r*) with confidence intervals, effect sizes, degrees of freedom and *P* value noted *Give P values as exact values whenever suitable.*
☒	☐	For Bayesian analysis, information on the choice of priors and Markov chain Monte Carlo settings
☒	☐	For hierarchical and complex designs, identification of the appropriate level for tests and full reporting of outcomes
☒	☐	Estimates of effect sizes (e.g. Cohen's *d*, Pearson's *r*), indicating how they were calculated

Our web collection on statistics for biologists contains articles on many of the points above.

Software and code

Policy information about availability of computer code

Data collection	Flow cytometry by using Novocyte (ACEA Biosciences) software (version 2000); quantitative PCR by using BIO-RAD CFX284TM Real-Time PCR Detection System; RNA-seq quality control and adapter trimming were accomplished using the FastQC (version 0.11.3) and Trim Galore (version 0.4.0) software packages, trimmed reads were mapped to the Genome Reference Consortium GRCm38 (mm10) murine genome assembly using TopHat2 (version 2.1.0), and feature counts were generated using HTSeq (version 0.6.1); 13C-tracer data by using Gas Chromatography-Mass Spectrometry (GC-MS) as standard method; medium metabolites by using Liquid Chromatography-Mass Spectrometry (LC-MS) (metabolon), NMR, or bioanalyzer (YSI, version 2900) as standard method; Oxygen consumption rate (OCR) by using seahorse XFe96 Analyzer (Agilent Technologies)
Data analysis	Flow cytomertric analysis were performed with FlowJo software (TreeStar, version 10.6); RNAseq analysis were performed using the DESeq2 package (version 1.16.1) in R, with the default Benjamini-Hochberg p-value adjustment method, the Ingenuity Pathway Analysis (IPA) software (QIAGEN, version 01-20-04), the Gene Set Enrichment Analysis (GSEA) software (UC San Diego, BROAD Ins. version 4.1.0), and the R Programming Language software (version 4.2.1); Oxygen consumption rate (OCR) were analysis by using the Seahorse Wave Software (Seahorse, Agilent Technologies. version 2.6); Statistical data analysis and generation of graphs by using GraphPad Prism (version 8.0.1).

For manuscripts utilizing custom algorithms or software that are central to the research but not yet described in published literature, software must be made available to editors and reviewers. We strongly encourage code deposition in a community repository (e.g. GitHub). See the Nature Portfolio guidelines for submitting code & software for further information.

Data

Policy information about availability of data

All manuscripts must include a data availability statement. This statement should provide the following information, where applicable:

- Accession codes, unique identifiers, or web links for publicly available datasets
- A description of any restrictions on data availability
- For clinical datasets or third party data, please ensure that the statement adheres to our policy

Raw RNA-seq datasets generated for this study can be found in the GEO accession GSE190818 (reserved released data at 08/02/2022). https://www.ncbi.nlm.nih.gov/geo/query/acc.cgi. The authors declare that all other data (including the Metabolon) and materials supporting the findings of this study are available within the article (and supplementary/ extended information files). Original LC-MS metabolomics data and code please address correspondence and requests for materials to Ruoning Wang (ruoning.wang@nationwidechildrens.org).

Field-specific reporting

Please select the one below that is the best fit for your research. If you are not sure, read the appropriate sections before making your selection.

☒ Life sciences ☐ Behavioural & social sciences ☐ Ecological, evolutionary & environmental sciences

For a reference copy of the document with all sections, see nature.com/documents/nr-reporting-summary-flat.pdf

Life sciences study design

All studies must disclose on these points even when the disclosure is negative.

Sample size	Sample sizes determined on the basis of previous experience in previous experiments. For Metabolon, LC-MS, GS-MS studies 3 independent samples for determination (referring Ratnikov, B. et al. Bioinfornatics 2006; Bunk, B. et al. Bioinfornatics 2006; Evans, A.M. et al. Anal Chem 2009); for EAE studies, 3-5 independent experiments with mice based on the experimental design (referring Wu, R. et al. Sci Adv 2020; Chen, X. et al. Sci Imm 2022); for Elisa, YSI, qPCR measurements, 3-6 independent samples were used; for in vivo adoptive transferred experiment, 3-5 independent mice were used (referring Wu, R. et al. Sci Adv 2020; Chen, X. et al. Sci Imm 2022); for cell culture related experiments such as FACS, 3 independent samples at least were performed. The number of independent experiments (at least 3) is a standard sample size to accurately detect differences in cell biology filed (referring multiple publications in Nature, Nature Metabolism, Nature Immunology, et al).
Data exclusions	No data exclusion
Replication	All experiments were conducted with at least two independent experiments and multiple biological replicates (except metabolon was performed one time and 3 biological replicates), and the details was provided in corresponding figure legends.
Randomization	All studies were performed on age and gender matched animals. Animals were randomized prior to experiments.
Blinding	Experiments were not performed blinded because all analysis were performed using same gating as control under the same condition.

Reporting for specific materials, systems and methods

We require information from authors about some types of materials, experimental systems and methods used in many studies. Here, indicate whether each material, system or method listed is relevant to your study. If you are not sure if a list item applies to your research, read the appropriate section before selecting a response.

Materials & experimental systems

n/a	Involved in the study
☐	☒ Antibodies
☒	☐ Eukaryotic cell lines
☒	☐ Palaeontology and archaeology
☐	☒ Animals and other organisms
☒	☐ Human research participants
☒	☐ Clinical data
☒	☐ Dual use research of concern

Methods

n/a	Involved in the study
☒	☐ ChIP-seq
☐	☒ Flow cytometry
☒	☐ MRI-based neuroimaging

Antibodies

Antibodies used	For cell culture: InVivoMAb anti-mouse CD3 (clone 145-2C11, Bio X Cell, Cat# BE0001-1) InVivoMAb anti-mouse CD28 (clone 37.51, Bio X Cell, Cat# BE0015-1) InVivoMAb anti-mouse IL-2 (clone JES6-1A12, Bio X Cell, Cat# BE0043)

InVivoMAb anti-mouse IL-4 (clone 11B11, Bio X Cell, Cat# BE0045)
InVivoMAb anti-mouse IFN gamma (clone XMG1.2, Bio X Cell, Cat# BE0055)
For flow cytometry: Anti-mouse CD4-FITC (clone RM4-5, Biolegend, Cat# 100510, dilution 1:100)
anti-mouse CD4-PE/Cyanine7 (clone GK1.5, Biolegend, Cat# 100422, dilution 1:100)
anti-mouse CD4-Pacific Blue (clone GK1.5, Biolegend, Cat# 100428, dilution 1:100)
anti-mouse CD8-APC/Cyanine7 (clone 53-6.7, Biolegend, Cat# 100714, dilution 1:100)
anti-mouse CD62L-APC (clone MEL-14, Biolegend, Cat# 104412, dilution 1:100)
anti-mouse CD44-FITC (clone IM7, Biolegend, Cat# 103006, dilution 1:100)
anti-mouse CD69-PE/Cy7 (clone H1.2F3, Biolegend, Cat# 104512, dilution 1:100)
anti-mouse CD25-PE (clone PC61, Biolegend, Cat# 102008, dilution 1:100)
anti-mouse CD45.1-PerCP (clone A20, Biolegend, Cat# 110726, dilution 1:100)
anti-mouse CD45.2-PerCP (clone 104, Biolegend, Cat# 109826, dilution 1:100)
anti-mouse Thy1.1-APC/Cy7 (clone OX-7, Biolegend, Cat# 202520, dilution 1:100)
anti-mouse Thy1.1-APC (clone OX-7, Biolegend, Cat# 202526, dilution 1:100)
anti-mouse Thy1.2-PE (clone 30-H12, Biolegend, Cat# 105308, dilution 1:100)
anti-mouse TCR beta-APC (clone GL3, Biolegend, Cat# 109211, dilution 1:100)
anti-mouse IFN gamma-APC (clone XMG1.2, Biolegend, Cat# 505810, dilution 1:100)
anti-mouse IFN gamma-PE/Cyanine7 (clone XMG1.2, Biolegend, Cat# 505826, dilution 1:100)
anti-mouse IL-17A-APC (clone TC11-18H10.1, Biolegend, Cat# 506916, dilution 1:100)
anti-mouse IL-17A-PE/Cyanine7 (clone TC11-18H10.1, Biolegend, Cat# 506922, dilution 1:100)
anti-mouse IL-4-APC (clone 11B11, Biolegend, Cat# 504105, dilution 1:50)
anti-mouse/human/rat ABAT-FITC or purified (clone B-12, Santa Cruz Biotechnology, Cat# sc-393769, dilution 1:50)
anti-mouse FoxP3-Alexa Fluor® 647 (clone MF-14, Biolegend, Cat# 126407, dilution 1:100)
anti-Hu/Mo ROR gamma (t) (clone AFKJS-9, eBioscience, Cat# 17-6988-82, dilution 1:50)
anti-Hu/Mo Phospho STAT3 (Tyr705) (clone LUVNKLA, eBioscience, Cat# 12-9033-42, dilution 1:50)
anti-Hu/Mo Phospho STAT5 (Tyr694) (clone SRBCZX, eBioscience, Cat# 12-9010-42, dilution 1:50)
P-S6Ribosomal Protein-Pacific Blue (S235/236) (clone D57.2.2E, Cell Signaling, Cat# 8520S, dilution 1:50)
anti-Alexa Fluro 647 BrdU (Biolegend, Cat# 364114, dilution 1:100)
Pyronin Y (Sigma-Aldrich, Cat# 92-32-0, dilution 1:100)

Validation

Reactivity of above antibodies are commercially available and validated for indicated applications, all information on manufacturer's homepage:
https://bxcell.com/
https://www.biolegend.com/
https://www.scbt.com/home
https://www.thermofisher.com/us/en/home/life-science/antibodies/ebioscience
https://www.cellsignal.com/
https://www.sigmaaldrich.com/US/en

Animals and other organisms

Policy information about studies involving animals; ARRIVE guidelines recommended for reporting animal research

Laboratory animals

C57BL/6 (WT), Flippase (B6.129S4Gt(ROSA)26Sortm1(FLP1)Dym/RainJ), OT-II (B6.Cg-Tg(TcraTcrb)425Cbn/J), CD45.1+ (B6.SJL-PtprcaPepcb/BoyJ), Rag1-/- (B6.129S7-Rag1tm1Mom/J), IL17A-IRES-GFP-KI (C57BL/6-Il17atm1Bcgen/J), FoxP3GFP+ (C57BL/6-Tg(Foxp3-GFP)90Pkraj/J), and Gabrb3fl (B6;129-Gabrb3tm2.1Geh/J) mice were obtained from the Jackson Laboratory (JAX, Bar Harbor, ME). Mice with one targeted allele of ABAT on the C57BL/6 background (ABATtm1a(EUCOMM)Hmgu) were generated by The European Conditional Mouse Mutagenesis Program (EUCOMM). The mice were first crossed with a transgenic Flippase strain (B6.129S4Gt(ROSA)26Sortm1(FLP1)Dym/RainJ) to remove the LacZ-reporter allele and then crossed with the CD4-Cre strain to generate T cell-specific ABAT knockout strain (ABAT cKO). OT-II mice were crossed with CD4Cre ABAT cKO mice to generate the OT- II CD4Cre ABAT cKO mice. OT-II mice were crossed with Thy1.1+ mice (B6.PL-Thy1a/CyJ) to generate the OT-II Thy1.1 mice. Gabrb3fl mice were crossed with the CD4-Cre strain to generate T cell-specific Gabrb3 knockout strain (Gabrb3 cKO). Both male and female mice, with age-matched (6-12 weeks old) were used in the experiments. Mice were housed under controlled conditions: rodent housing rooms are kept at 73 degree Fahrenheit, with alarms set at 69 and 78 degrees, 30–70% relative humidity, and 12:12 light-dark cycle. Food and water was available for all animals. Low Fat diet were provided (Envigo 2920, the irradiated form of 2020X*). Mice were maintained and euthanized (by carbon dioxide asphyxiation followed by cervical dislocation) under protocols approved by the Institutional Animal Care and Use Committee of the Research Institute at Nationwide Children's Hospital (IACUC; protocol number AR13-00055). *https://insights.envigo.com/hubfs/resources/data-sheets/2020x-datasheet-0915.pdf

Wild animals

This study does not include any wild animal.

Field-collected samples

This study does not include samples collected from the field.

Ethics oversight

Animal protocols were approved by the Institutional Animal Care and Use Committee of the Research Institute at Nationwide Children's Hospital.

Note that full information on the approval of the study protocol must also be provided in the manuscript.

Flow Cytometry

Plots

Confirm that:

☒ The axis labels state the marker and fluorochrome used (e.g. CD4-FITC).

☒ The axis scales are clearly visible. Include numbers along axes only for bottom left plot of group (a 'group' is an analysis of identical markers).

☒ All plots are contour plots with outliers or pseudocolor plots.

☒ A numerical value for number of cells or percentage (with statistics) is provided.

Methodology

Sample preparation	For development analysis, spleen, lymph nodes and thymus were passed through 70 micron filters; for EAE infiltrating T cell analysis, the CNS (brain and spinal cord), spleen, and peripheral lymph nodes were collected and mashed to make the single-cell solution. The cell suspension was centrifuged on a 30%/70% Percoll gradient at 500 g for 30 min to isolate mononuclear cells from the CNS. All cells were stained in PBS containing 2% (w/v) BSA and the appropriate antibodies from Biolegend. For analyzing intracellular cytokine IFN-gamma and IL-17A, T cells were stimulated for 4 hrs with eBioscience™ Cell Stimulation Cocktail (eBioscience) before being stained with cell-surface antibodies. Cells were then fixed and permeabilized using FoxP3 Fixation/ Permeabilization solution according to the manufacturer's instructions (eBioscience). Cell proliferation was assessed by CFSE staining per the manufacturer's instructions (Invitrogen). Cell viability was evaluated by 7AAD staining per the manufacturer's instructions (Biolegend). For analyzing DNA/RNA content, cells were collected and stained with surface markers before being fixed with 4% paraformaldehyde for 30 min at 4°C, followed by a step of permeabilization with FoxP3 permeabilization solution (eBioscience). Cells were stained with 7AAD for 5 min and then stained with pyronin-Y for 30 min before being analyzed by flow cytometer with PerCP channel for 7AAD (DNA) and PE channel for pyronin-Y (RNA). Protein synthesis assay kit (Item No.601100, Cayman) was used for analyzing protein content. Briefly, cells were incubated with O-propargyl-puromycin (OPP) for 1 hr, then were fixed and stained with 5 FAM-Azide staining solutions before being analyzed by flow cytometer with FITC channel. For analyzing cell cycle profile, cells were incubated with 10 μg/mL BrdU for 1 hr, followed by cell surface staining, fixation, and permeabilization according to Phase-Flow Alexa Fluro 647 BrdU Kit (Biolegend).
Instrument	Novocyte
Software	FlowJo version 10.6
Cell population abundance	Bulk cell isolation including naive CD4 T cells and naive tTreg cells were performed using kits (MojoSort, BioLegend) individually, ensuring a purity of >90%-95% defined as the ratio of target cells and total cells. For RNAseq, WT and ABAT cKO T cells were activated and harvested at 36 hrs separately, used for RNA extraction (around 100-500 ng/ul/sample). For Metabolon assay, differentiated CD4 subsets such as TH1, TH17 and iTreg for 72 hrs, FACS determined to ensure a purity of about 70% defined as the ratio of IFN gamma (TH1), IL17A (TH17) and FoxP3 (iTreg) and total cells. For in vitro Treg cell suppression assays, differentiated iTreg for 72 hrs, FACS determined to ensure a purity of about 70% FoxP3 (iTreg) cells, co-cultured with Tconv cells in indicated ratio as described in Methods. Brifely, purity of cell fractions were determined by flow cytometry ensuring a appropriate purity based on the experiment purpose. No cell sorting were performed at this time.
Gating strategy	Gating strategies are shown respectively: For analysis of alive cells (Fig 2j, Fig 5b, Fig 5e, Fig S3a, Fig S3e, Extended Data Fig 9a, and Fig 9b): PerCP-7AAD gating for alive cells (Fig 2j upper) followed by analysis of GFP-surface expressed IL17A, or detected CFSE cell proliferation, or CD25/CD69 cell activation marker; for analysis of CD4+ T cell proliferation, infiltrating and intracellular cytokines (Fig 4c, Fig 4g, Fig 4i, Fig 4k, Fig 5f, Fig 5h, Extended Data Fig 2b, Fig 4a-d, Fig 5, Fig 6b, Fig 8b, Fig 9c, and Fig 10): FSC-SSC-H gating was used as preliminary gating for lymphocyte population followed by analysis of CD4+ T cells, then checked the intracellular cytokines expression (gating strategy in Supplementary Information); for in vivo adaptive transfer experiment, gating strategy for flow cytometry analysis was preliminarily performed by gating for CD45.2 stain marker (Extended Data Fig 6a, OVA antigen-specific), by gating for TCR-beta (Extended Data Fig 6d, homeostatic), and then checked the cell ratio, proliferation or cytokines expression; for Treg cell suppression assay, gating strategy for flow cytometry analysis was preliminarily performed by gating for CD45.2 stain marker to distinguish the Tconv cells, then separated WT cells and KO cells by Thy1.1 marker and Thy1.2 marker (Fig 6e), and then checked the proliferation.

☒ Tick this box to confirm that a figure exemplifying the gating strategy is provided in the Supplementary Information.